Bioorganic Chemistry 109 (2021) 104729

Contents lists available at ScienceDirect

Bioorganic Chemistry

journal homepage: www.elsevier.com/locate/bioorg

Novel thienopyrimidine analogues as potential metabotropic glutamate receptors inhibitors and anticancer activity: Synthesis, *In-vitro*, *In-silico*, and SAR approaches

Mohammed A. Khedr [a,*], Khadiga M. Abu-Zied [b], Wafaa A. Zaghary [a,*], Ahmed S. Aly [b], Dina N. Shouman [c], Hesham Haffez [d,e]

[a] Department of Pharmaceutical Chemistry, Faculty of Pharmacy, Helwan University, P.O. Box 11795, Cairo, Egypt
[b] Photochemistry Department (Heterocyclic Unit), National Research Centre, Dokki, Giza 12622, Egypt
[c] Family Medicine Center, Egyptian Ministry of Health and Population, Dakahlia, Egypt
[d] Biochemistry and Molecular Biology Department, Faculty of Pharmacy, Helwan University, P.O. Box 11795, Cairo, Egypt
[e] Center of Scientific Excellence "Helwan Structural Biology Research, (HSBR)", Helwan University, Cairo 11795, Egypt

ARTICLE INFO

Keywords:
Thienopyrimidines
Anticancer
Apoptosis
Docking
Molecular dynamics
mGluR-1 inhibitor

ABSTRACT

There is a continuous need in drug development approach for synthetic anticancer analogues with new therapeutic targets to diminish chemotherapeutic resistance of cancer cells. This study presents new group of synthetic thienopyrimidine analogues (**1**–**9**) aims as mGluR-1 inhibitors with anticancer activity. *In-vitro* antiproliferative assessment was carried out using viability assay against cancer cell lines (MCF-7, A-549 and PC-3) compared to WI-38 normal cell line. Analogues showed variable anticancer activity with IC_{50} ranging from 6.60 to 121 μg/mL with compound **7b** is the most potent analogue against the three cancer cell lines (MCF-7; 6.57 ± 0.200, A-549; 6.31 ± 0.400, PC-3;7.39 ± 0.500 μg/mL) compared to Doxorubicin, 5-Flurouracil and Riluzole controls. Selected compounds were tested as mGluR-1 inhibitors in MCF-7 cell line and results revealed compound **7b** induced significant reduction in extracellular glutamate release (IC_{50}; 4.96 ± 0.700 μM) compared to other analogues and next to Riluzole (IC_{50}; 2.80 ± 0.500 μM) of the same suggested mode of action. Furthermore, both cell cycle and apoptosis assays confirmed the potency of compound **7b** for early apoptosis of MCF-7 at G_2/M phase and apoptotic positive cell shift to (91.4%) compared to untreated control (19.6%) and Raptinal positive control (51.4%). On gene expression level, compound **7b** induced over-expression of extrinsic (FasL, TNF-α and Casp-8), intrinsic (Cyt-C, Casp-3, Bax) apoptotic genes with down-regulation of anti-apoptotic Bcl-2 gene with boosted Bax/Bcl-2 ratio to 2.6-fold increase. Molecular docking and dynamic studies confirmed the biological potency through strong binding and stability modes of **7b** where it was faster in reaching the equilibrium point and achieving the stability than Riluzole over 20 ns MD. These results suggest compound **7b** as a promising mGluR inhibitory scaffold with anticancer activity that deserves further optimization and in-depth *In-vivo* and clinical investigations.

1. Introduction

Current available cancer drug therapy in market are antimetabolites and alkylating agents that traditionally based on targeting DNA synthesis and cell division [1]. Although these traditional therapies show efficacy against broad spectra of cancer types, the lack of selectivity and specificity over normal cells can lead to severe side effects [2]. Increasing the knowledge and understanding new particular targets and their correlation with cancer, opened the gate for new era of rational and targeted approaches in cancer treatment [3]. One of these selected targets is glutamate, a well-characterized excitatory neurotransmitter in mammals involved in nociception and pain sensitization [4], arthritis [5], polymyalgia [6] and other inflammatory disorders [7]. It is a cell-signaling molecule found mainly in both central nervous system (CNS) and periphery tissues such as bone, spleen, lung, pancreas, heart, liver [8]. Function of glutamate is mediated by binding to either ionotropic or metabotropic receptors on cell surface [9]. Metabotropic glutamate receptors types (mGluR-1 to mGluR-8) belong to the family of G-protein-

* Corresponding authors.
E-mail addresses: mohammed_abdou@pharm.helwan.edu.eg (M.A. Khedr), Wafaa.zaghary@pharm.helwan.edu.eg (W.A. Zaghary).

https://doi.org/10.1016/j.bioorg.2021.104729
Received 7 November 2020; Received in revised form 12 January 2021; Accepted 6 February 2021
Available online 16 February 2021

coupled seven transmembrane domain receptors (GPCRs) [10] that plays key role in synaptic signaling and mental performance [11]. Another specific controller of cysteine and glutamate transport is heteromeric, sodium-independent, anionic amino acid transport system referred as Xc(-) and coded by gene called SLC7A11 [12]. Cysteine is transported in exchange for glutamate [13] that was identified as predominant mediator for entry and fusion of herpesvirus associated with Kaposi sarcoma [14]. Recent data showed mGluRs and especially type-1 plays key role as pro-angiogenic factor regulating breast cancer cell proliferation and tumor growth [8,9]. mGluR-1 and SLC7A11 were demonstrated to be over-expressed and responsible for tumorigenesis in different cancer types such as melanoma [15,16], gliomas [15] by increasing proliferation [15,17], angiogenesis [15], metastatic [18] and aggressiveness phenotypes of these cancer cells. In addition to glutamate exchange system, intracellular glutamate was observed as a primarily source from glutamine metabolism in cancer cells with a proportion of this glutamate is secreted extracellularly [8,19]. Both dysregulated glutamatergic signaling pathway and over-secretion of glutamate have been shown to correlate with worsening malignant phenotype [8,9]. Using mGluR-1 targeted knockdown model by shRNA using viral constructs has been shown to inhibit proliferation of cancer cells compared to non-silencing controls and it was the first in literature to confirm the role of mGluRs as new anticancer therapeutic target [9]. Riluzole (Fig. 1) was the first FDA-approved drug as glutamate receptors antagonist designed specifically for mGluR-1 [20] and used as anticonvulsant to improve the survival rate of amyotrophic lateral sclerosis patients [21]. Recent investigations aimed to repurpose it for the treatment of different cancers since it was demonstrated to inhibit cellular growth and tumorigenesis in many cancer types such as breast cancer [22], melanoma [22], glioma [23], and prostate cancer [24]. However, Riluzole has different associated severe side effects such as decreased lung function, muscle tremors and feeling of pins and needles pain sensation on skin [25]. In addition, due to lack of specificity to cystine/glutamate transporter (xCT) and glutamate release, Riluzole might harm normal and stem-like cell metabolism, energy production and proliferation making its effect is controversial [26,27]. Another examples of mGluR1 antagonists with anticancer that was approved is (S)-4-Carboxyphenylglycine that acts originally as anticonvulsants and antiepileptogenic agent [28]. Fig. 1 shows other new bioactive synthetic analogues with diverse mGluRs inhibitory activity on different mGluR-types with biological activity including anticancer [29]. Synthetic thienopyrimidines are class of bioactive compounds with wide range of biological activities such as antimicrobial [30], anti-inflammatory [31], antihistaminic [32], anticonvulsant [33] and immunostimulant [34] properties. Thienopyrimidine have received considerable attention for their mGluRs inhibition with potential anticancer activity. Based on the previously mentioned findings and synthetic scaffolds, newly substituted thienopyrimidine derivatives aims mGluR-1 inhibition were synthesized and evaluated for their anticancer activity against different cancer cell lines (MCF-7, A-549 and PC-3) compared to normal cell line WI-38. Top ranked selected series of the tested compounds will be further explored on the sensitive cancer cell line for their mGluR-1 inhibitory activity and to correlate with anti-proliferation activity. Finally, the inhibitory effects of the most potent analogue(s) were investigated by molecular docking and dynamic studies to predict and explain their binding mode and stability toward mGluR-1 inhibition as a possible new mechanism of the action for these new synthetic analogues.

2. Results and discussion

2.1. Chemistry

2.1.1. Design of the target compounds

Our target compounds were designed depending upon the following proposed design in Fig. 2 in which the 5-Isopropyl-6-methylthieno[2,3-*d*]pyrimidin-4(3*H*)-one scaffold was retained. Different substitutions on the 2-thiol group were performed to evaluate their effect.

The synthetic pathways adopted for the preparation of the intermediates and the target compounds were depicted in Schemes 1–5. The starting material ethyl 2-amino-4-isopropyl-5-methylthiophene-3-carboxylate **1** was prepared according to Karl Gewald reaction (version **II**) which consider the easiest and fluent method [35,36]. It was applied by two ways; A **stepwise reaction**, include reaction of methyl isobutyl ketone with ethyl cyanoacetate and diethyl amine in absolute ethanol and addition of sulfur powder portion wise result in compound **1** in low yield. Another way, a **one-pot reaction** that include to add all sulfur powder to liquid mixture at once. The shiny grey crystals produced in good yield. The spectral data, TLC and (m.p. 98–100 °C) of compound **1** prepared with this method, was compatible with that obtained from the first method, See experimental (Scheme 1).

Scheme 2 showed reaction of compound **1** with potassium thiocyanate in dry dioxane and concentrated HCl result in compound **2′**. ^{13}C NMR (DMSO-d_6) showed characteristic signals at δ 174.6 *ppm* corresponding to (C═S) indicating the obtained acyclic thione structure. On

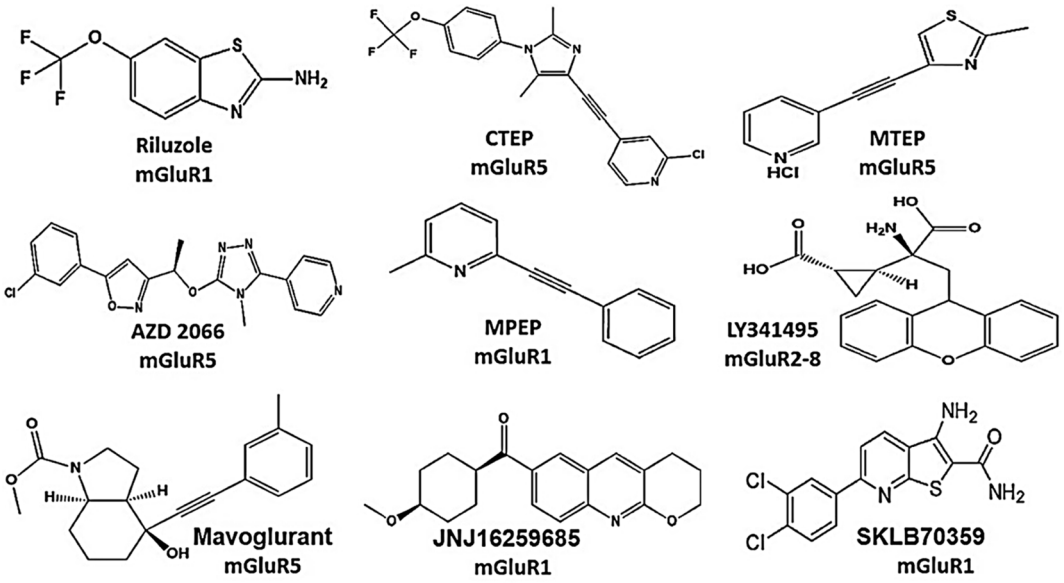

Fig. 1. Examples of synthetic mGluRs antagonists with diverse biological activity including Riluzole.

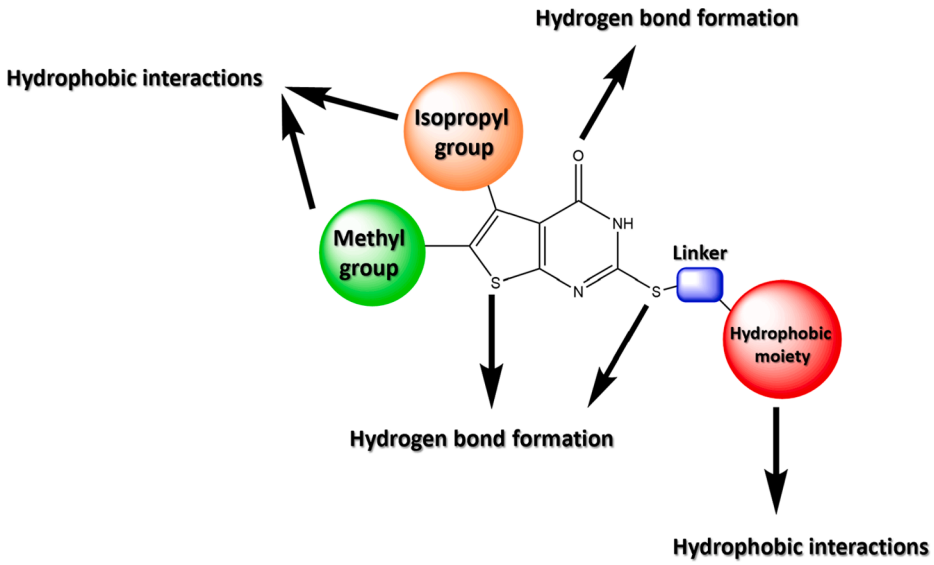

Fig. 2. Proposed design of the target compounds.

other hand, when compound **2′** treated with NaOH 5% solution and then neutralized with concentrated HCl, the closed thione **2** was obtained. The IR-spectrum of **2** showed no band corresponding to NH_2 group. Also a band at 1653 cm^{-1} appear (corresponding to amidic carbonyl) instead of ester carbonyl at 1720 cm^{-1}, See experimental.

A series of 6-isopropyl-7-methyl-5*H*-thiazolo[3,2-*a*]thieno[2,3-*d*] pyrimidine-3,5(2*H*)-dione derivatives **5 a-c** synthesized by two methods; either from compound **2** or from compound **3**.

Compound **3** was prepared by heating under reflux a mixture of **2** with chloroacetic acid, anhydrous sodium acetate, glacial acetic acid and acetic anhydride that afford to formation of compound **3**. On heating under reflux compound **3** with an appropriate aromatic aldehydes used as; 4-methoxybenzaldehyde, indole-3-carboxaldehyde and 4-hydroxy-3-nitrobenzaldehyde in the presence of anhydrous sodium acetate, glacial acetic acid and acetic anhydride, **5a-c** were obtained **(Two-step reaction)**.

For **one-pot reaction**, addition a mixture of compound **2** with chloroacetic acid, anhydrous sodium acetate, glacial acetic acid, acetic anhydride and different aldehydes used like 4-methoxybenzaldehyde, indole-3-carboxaldehyde or 4-hydroxy-3-nitrobenzaldehyde afford to the corresponding compounds **5 a-c**. The structures of the newly obtained compounds are confirmed through different spectral and elemental data.

IR spectrum of **5a** compound give no absorption bands at NH region. Also, it show two amidic carbonyl bands at 1671, 1652 cm^{-1}, while ^{1}H NMR (DMSO-d_6) spectrum showed no signal at δ 3.87 *ppm* indicate the absence of CH_2 (active methylene group) and no signal at δ 10.28 *ppm* corresponding to NH group and the appearance of signals at δ 3.87 for ($-OCH_3$), δ 7.31 *ppm* (d, $J = 8$ Hz, 2H, Aromatic protons), δ 7.89 *ppm* (d, $J = 8$ Hz, 2H, Aromatic protons), δ 8.03 *ppm* (s, 1H, methine proton) indicating the presence of aromatic moiety in **5a**.

Notice that using both of 4-methoxybenzaldehyde and indole-3-carboxaldehyde the reaction need more heating hours than the third aldehyde (4-hydroxy-3-nitrobenzaldehyde).

Furthermore, synthesis of derivatives **7 a-d** was achieved by heating of ethanolic potassium hydroxide solution and compound **2** under reflux, then add various alkylating agents namely, chloroacetic acid, ethyl chloroacetate, phenacyl bromide, and iodomethane. The precipitate obtained dried and crystallized from proper solvent that afford to corresponding derivatives **7 a-d**. IR-spectrum data for compound **7a** as an example showed absorption bands at 3430 cm^{-1} (broad peak for OH group), 3140 cm^{-1} for (NH group) and 1721 and 1657 cm^{-1} for two carbonyl groups (C═O).

^{1}H NMR (DMSO-d_6) spectra showed signals at δ *4.02 ppm* for CH_2 group, and at δ 12.74 *ppm* indicate the presence of OH group. and at δ 10.71 *ppm* (for NH group). Also ^{13}C NMR (DMSO-d_6) showed signals at δ 168.8 *ppm* (C═O) and at δ 172.0 *ppm* (COOH) **(**Scheme 4**)**.

Heating under reflux compound **7d** with hydrazine hydrate (99%) with ratio (1:3), in the presence of absolute ethanol and dioxane (1:1). The formed product dried and recrystallized from solvent that gave compound **8**, in its enol form which unexpected result [35–37].

The structure of obtained enol form **8** confirmed by IR-spectrum at 3441 cm^{-1} (broad peak for OH) instead of carbonyl band corresponding to the enol form and at 3245, 3201 cm^{-1} for (NH_2 group), and 3140 cm^{-1} for (NH), while ^{1}H NMR (DMSO-d_6) spectra confirm the enol form by the presence of peaks at δ 6.95 *ppm* for NH_2, and at δ 12.58 *ppm* corresponding to OH group. Also ^{13}C NMR (DMSO-d_6) spectrum showed no absorption peak of carbonyl region.

Mixture of compound **8**, few drops of piperidine, absolute ethanol, and 4-fluorobenzaldehyde, was heated under reflux. The formed product was dried and recrystallized from ethanol to obtain compound **9**.

The IR-spectra of compound **9** showed broad peak at 3434 cm^{-1} for (OH group) corresponding to enol form not for keto form, and no absorption band for NH_2 group, while ^{1}H NMR (DMSO-d_6) showed signals at δ 7.02 *ppm* (dd, $J = 35$, 10 Hz, 2H, for aromatic protons), δ 7.64 *ppm* (d, $J = 10$ Hz, 2H, for aromatic protons), δ 8.07 *ppm* (s, 1H, methine proton) and at δ 12.50 *ppm* for OH group **(**Scheme 5**)**.

2.2. Biological evaluation

2.2.1. In-vitro antiproliferative and cytotoxicity activity

Table 1 showed the *In-vitro* antiproliferative (viability) assay of the target compounds (**1–9**) which were evaluated against three human cancer cell lines including MCF-7 (human breast cancer cells), A-549 (adenocarcinoma human alveolar epithelial cells), PC-3 (human prostate cancer cell line**)**, and WI-38 normal human fibroblast cell line using MTT assay and Doxorubicin, 5-Fluoruracil and Riluzole as positive controls. The results showed that synthetic thienopyrimidine compounds exhibited variable antiproliferative activity with IC_{50} in the range of 6.57 –198 μg/mL against all tested cancer cell lines. The compounds were classified according to their potency of IC_{50} value into three major categories [38,39] (Table 1): category (1) less than 10 μg/mL, category (2) (10.0–50.0 μg/mL) and category (3) > 50 μg/mL. Compounds **7a** with (thio-acetic acid substitution) and **7b** (Ethyl-2-thioacetic acid substitution**)** showed most potent antiproliferative activity against all tested cancer cell lines with IC_{50} less than 10.0 μg/mL; MCF-7

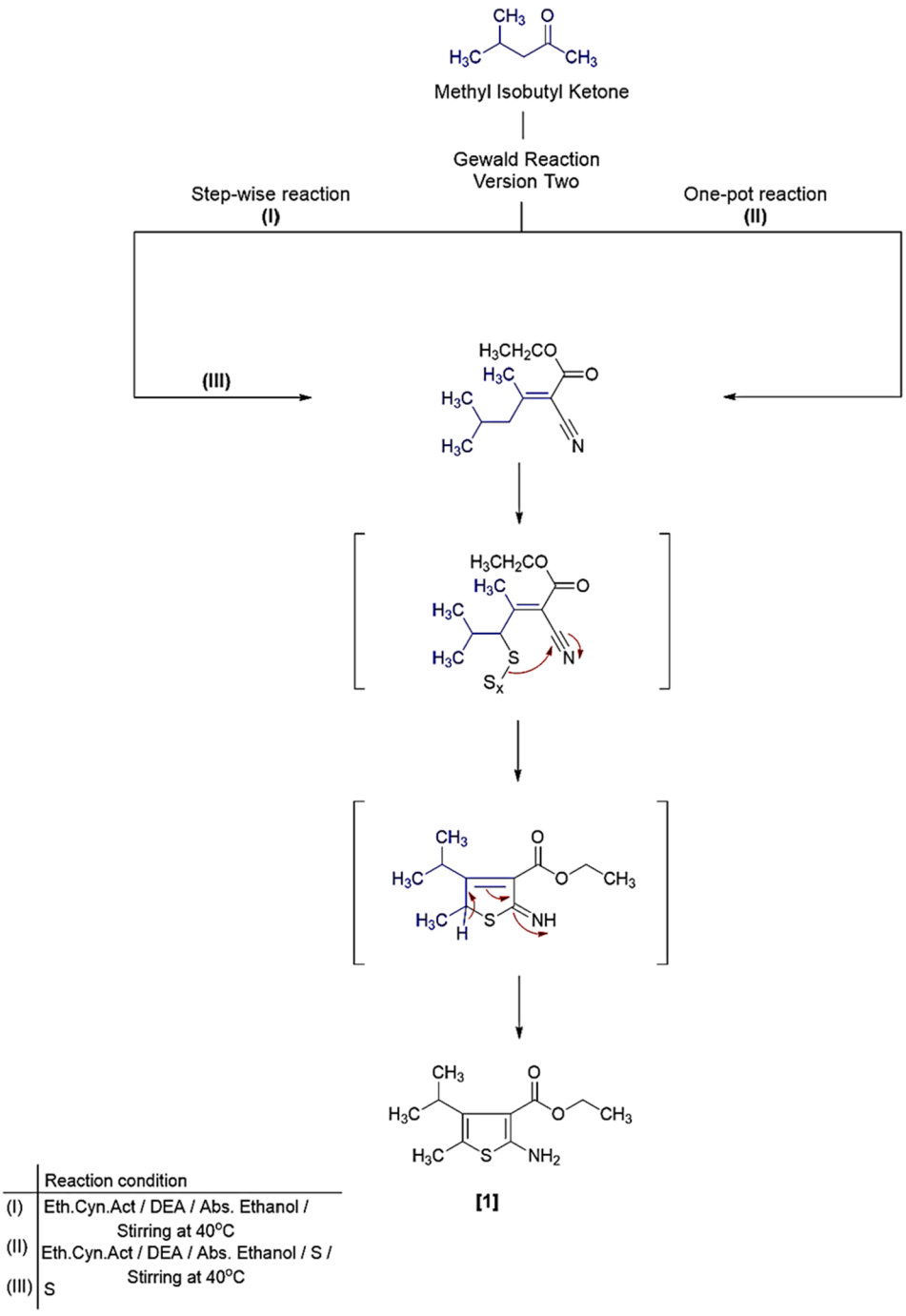

Scheme 1. Proposed mechanism of compound **1** formation.

(7.50 ± 0.300 and 6.57 ± 0.200 μg/mL respectively), A-549 (6.42 ± 0.700 and 6.31 ± 0.400 μg/mL respectively), and PC-3 (11.3 ± 0.900 and 7.39 ± 0.500 μg/mL respectively), stronger than those of positive controls. Compounds **1** (ethyl-2-amino-4-isopropyl-5-methyl-thiophene-3-carboxylate), **1′**, **2** with (2-mercapto) group, **3** with (Thiazolo [3,2,*a*] thieno [2,3, *d*] pyrimidine-3,5 (2*H*) dione**, 7c** that has (2-(2-oxo-2-phenyl ethyl) moiety, **8** with (3-hydrazinyl) group, **4b** that has (3-*H*-indol-3-yl) thio acrylic acid, **5b** with (2-((1*H*-indol-3-yl)methylene and **9** with (2-(2-(4-fluorobenzylidene) hydrazinyl) substitution showed good to moderate antiproliferative activity with IC_{50} values (10.0–50.0 μg/mL) against two of the tested cancer cell lines (MCF-7 and A-549) slightly higher than that of standard controls. Finally, compounds **2′** with (2-thioreidothiophene-3-carboxylate) substitution, **4a** that has (thio-3-(4-methoxy phenyl) acrylic acid moiety, **5a** with (2-(4-methoxy benzylidene) group, **7d** with (2-methyl thio) substitution and **5c** that possess (2-(4-hydroxy-3-nitrobenzylidene) group showed least anti-proliferative activity with IC_{50} values > 50.0 μg/mL against all tested cancer cell lines and compared to positive controls. Also, the cytotoxicity of the synthetic thienopyrimidine compounds were assessed against normal cells using WI-38 cell line with the calculation of selectivity index (SI) values. All of the synthetic compounds in the categories (1) and (2) showed no significant cytotoxicity to normal cells comparable to the standard positive controls with SI values more than 1 where the higher the SI, indicates more effective and safer compound would be [39,40]. The highest SI values were for compounds **7a** and **7b** while compounds with category (3) showed the least SI values (less than 1) compared to positive controls.

Based on the observed results, compounds **7a** and **7b** were the most

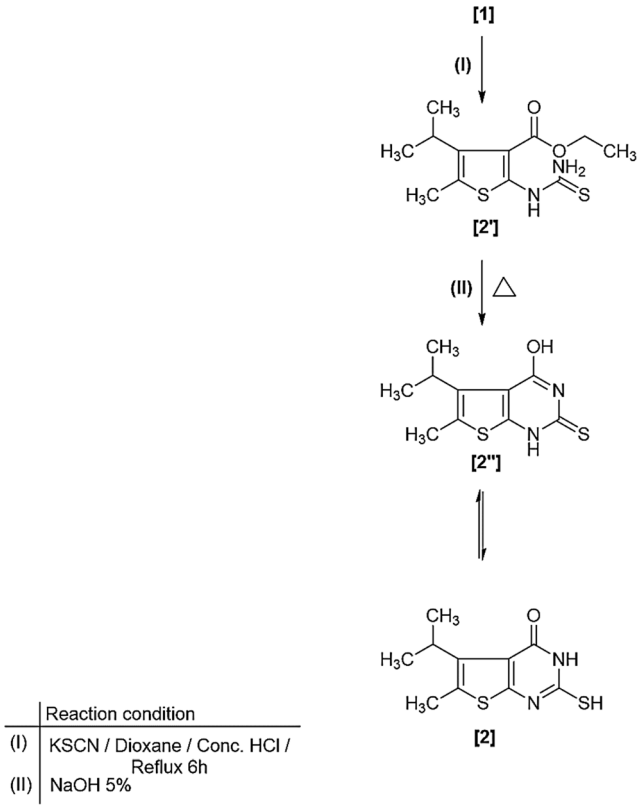

Scheme 2. Synthetic pathway for compound **2** with its tautomer.

potent antiproliferative compounds with safer margin for cytotoxicity compared to standard chemotherapeutic agents (Doxorubicin and 5-Flurouracil) as well as Riluzole of the same suggested class of compounds and mechanism of action. Additionally, one-third of tested compounds approximately showed moderate antiproliferative activity with safe margin for cytotoxicity. This may suggest **7a** and **7b** are promising candidates for further biological assessment in comparison to thienopyrimidines from the other categories to understand possible effect on mGluR-1 and anticancer activity. MCF-7 cell line was sensitive cell line for Riluzole standard drug with comparable results to both **7a** and **7b** and will be selected for further biological investigations.

2.2.2. Glutamate inhibitory assay

Concentration of extracellular and intracellular glutamate measured by this assay can be used to understand if the mechanism of antiproliferative activities of these active thienopyrimidine compounds may be mediated due to inhibition of mGluRs [41]. Glutamate is one of the paracrine mediators affecting intracellular communications and any small changes in its levels can lead to abnormal cellular transformation and cancer progression [42,43]. Several studies showed that extracellular glutamate secreted by cancer cells such as MCF-7 can induce paracrine effect on neighbour cells leading to tumour expansion and metastasis [9,44]. Hence, mGluR-1 particulary was sugessted as the major sub-type of glutamate receptor present in cell surface of breast cancer MCF-7 cell line and other cell lines that play critical role in tumour progression [45].

Additionally, mGluR-1 expression was examined in transgenic cancer animal model and it was detectable in tumor but not normal samples [46]. Therfore, recent attention has been given to this type of receptor in new era of drug development plans to link breast cancer resistence with chemotherapeutic efficiency [23] and apoptosis [47]. This evidence in literature suggests that both mGluRs and glutamate can play potential role as diagnostic and therapeutic targets [48,49] and consequently, their inhibition will affect significantly cell viability, invasion and migration [23]. IC_{50} of glutamate release inhibitory activity was measured by the ability of the tested theinopyrimdine analogues to reduce 50% of the glutamate released extracellulary compared to negative control MCF-7 cells treated with 0.1% DMSO solvent. Thienopyrimdine tested analogues were selected as follow; **7a** and **7b** from category (1), **1′**, **2**, **3**, **7c**, **8**, **4b**, **5b** and **9** from category (2) and **4a**, **5a** and **5c** from category (3) were selected as representative compounds for the further assesment in glutamate inhibitory activity assay. Riluzole was co-assayed as positive control of known activity for inhibition of mGluR-1 and glutamate release in MCF-7 cell line [20,21]. IC_{50} values for the tested analogues were calculated from the dose response curve presented in Fig. 3. Table 2 revealed that most of the tested compounds displayed variable levels of glutamate release inhibition except **4b** with (*H*-indol-3-yl) thio acrylic acid moiety, **5b** with (2-((1*H*-indol-3-yl) methylene group and **9** with (2- (2-(4-fluorobenzylidene) moiety that did not show any inhibitory activity over the tested series concentrations. Exceptionally, thienopyrimidine analogue **7b** with (Ethyl-2-thio acetic acid) substitution exhibited the most potent inhibitory activity against glutamate release in dose-dependent matter relative to other thienopyrimidines with IC_{50} (4.96 ± 0.700 μM) next to IC_{50} of Riluzole (2.80 ± 0.500 μM) and consequently suggested to have inhibitory activity to mGluR-1 inducing antiproliferation activity. Next, it was essential to use the IC_{50} doses from Table 2 measured for these thienopyrimidine analogues to measure intracellular glutamate level as shown in Table 3. Data presented in Fig. 4 showed that compound **7c** with (2-((2-oxo-2-phenylethyl)thio) group only showed significant elevated level of intracellular level of glutamate (37.1 ± 7.00 μM) compared to Riluzole (32.2 ± 5.00 μM). Compounds **7a** (thio acetic acid group) and **7b** (Ethyl-2-thio acetic acid group) did not show significant elevation of intracellular glutamate release in similar behaviour (31.7 ± 5.00 μM) compared to Riluzole. This difference in activity may explain the moderate antiproliferation for the tested compound **7c** based on its ability to increase intracellular glutamate level. Recent data from literature showed that accumulation of intracellular glutamate is shown to be toxic to cells since it will alter the different intracellular metabolic signaling pathways and favor the formation of glutamine through glutamine synthase rather than α-ketogluterate [50]. This has consequences of events on cancer cells include disrupted glycolysis and TCA cycle that will deprived cancer cells from rapid growth and proliferation [51]. Moreover, effect on glycolysis and TCA will reduce intermediates essential for cancer cell growth and biosynthesis of important molecules as nucleic acids, proteins, lipids and NAD^+/NADH redox balance [52]. Therfore, cancer cells will undergo forced ATP energy production mainly through oxidative phosphorylation with higher potential for reactive oxygen species (ROS) production [50]. Simillar case in literature with Glioma cells when intracellular Glu levels rise with inhibition of mGluR-1, the glutamine/cysteine antiporter System x^-_c was impaired and so cysteine as a major component of the antioxidant Glutathione (GSH) biosynthesis was depleted leaving cancer cells reliable for ROS and triggerring apoptosis [53]. Therefore, glutamate assay is considered an efficient tool to hypothesize the differential activity of two compounds such as **7b** and **7c** where the former inhibits extracellular glutamate release and mGluR-1 while the latter increases intracellular glutamate with all these data presented suggest that modulation in glutamate release and intracellular accumulation is acting as a good promising candiate of anticancer activity.

2.2.3. Cell cycle analysis

mGluR-1 inhibitors are known to induce cell cycle arrest through (G_2/M phase) [21,23,54]. It was essential to explore the efficacy of selected thienopyrimidine analogues for induciton of cell cycle arrest, compared to Raptinal as positive control in this experment since it was documented for its potent antiproliferative and apototic effect [55,56]. The most potent thienopyrimidine analogues from viability assay; **7a**, **7b** and the least potent analogue **5c** were tested to investigate whether their m-GluR-1 inhibitory effect on MCF-7 cell death leads to cell cycle

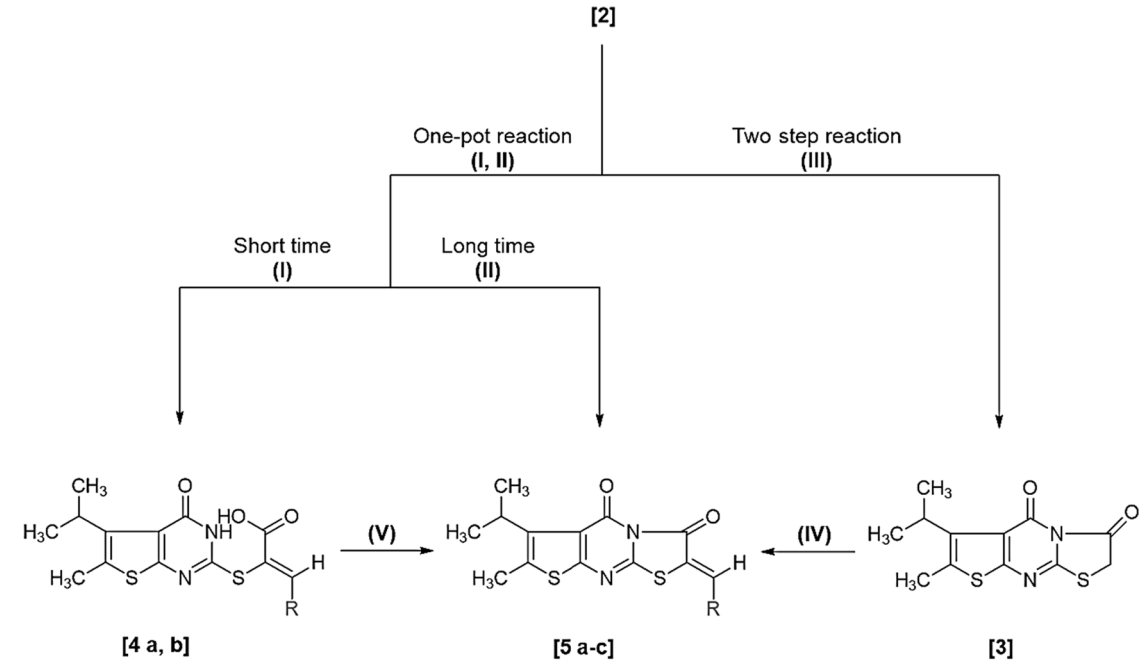

	Reaction condition
(I)	Cl.Ac.Ac./ Na Acet.(Anh) / G.Ac.Ac. / Ac.Anh / R-CHO
(II)	Cl.Ac.Ac./ Na Acet.(Anh) / G.Ac.Ac. / Ac.Anh / R-CHO
(III)	Cl.Ac.Ac./ Na Acet.(Anh) / G.Ac.Ac. / Ac.Anh
(IV)	R-CHO
(V)	Cl.Ac.Ac./ Na Acet.(Anh) / G.Ac.Ac. / Ac.Anh

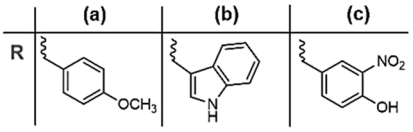

Scheme 3. Chemical synthesis of compounds; **3**, **4a, b**, and **5a-c.**

arrest. Propedium iodide (PI) staining assay was performed on MCF-7 treated cancer cells using flow cytometry and all tested compounds were used in IC_{50} dose obtained from MTT assay for 24 hrs. Fig. 5 showed that percentages of arrested MCF-7 cells treated with **7a**, **7b** and **5c** were significantly accumulated in the G_2/M phase than those in the control MCF-7 cells treated with 0.1% DMSO (**7a**; 98.8%, **7b**; 98.9%, **5c**; 98.8% and control 0.1%DMSO; 1.70%, Table 4). The mode of cell cycle arrest of the selected synthetic thienopyrimidines at G_2/M phase is similar to Raptinal treated cells (99.2%). Moreover, there was normal distribution of cells in the G_0-G_1- and S-phases in all tested cells compared to the negative control (Table 4) indicating no obvious effect on cells in these phases. Previous studies showed that thienopyrimidines with inhibitory activity to glutamate release and anticancer activity were arresting cancer cells during the mitotic phase [57–60]. This observation was consistent with data presented and might provide a possible explanation of cell cycle arrest observed at G_2/M phase in cells treated with tested thienopyrimidines especially **7b**.

2.2.4. *Apoptosis assay (Annexin-V staining assay)*

To evaluate the stage and potency of cell death induced by thienopyrimidine analogues, annexin-FITC/propidium iodide (PI) staining assay was performed in MCF-7 cells. This assay enables the detection of stage of apoptosis due to compound treatment presented in different 3D-plot quadrants, as live cells (bottom left quadrant), early apoptotic cells (bottom right quadrant), late apoptotic cells (top right quadrant) and necrotic cells (top right quadrant) [61,62].

Fig. 6 showed the distribution of cells at each stage (quadrant) for determination of apoptotic potency of compounds with overlayed histograms. **7b** (exhibiting the highest antiproliferative activity in MCF-7 cancer cells) showed significant increase of total early apoptotic cells to 91.4% compared to Raptinal treated cells (51.4%), **7a** (68.9%), **5c** (78.8%), negative control (1.63%), Table 4. Moreover, compound **7b** significantly reduced the percentage of viable cells (8.5%) compared to negative control (80.3%). This effect was potent enough than other analogues (**7a**; 31.1%, **5c**; 21.1%) and positive control of Raptinal (48.6%). Necrosis is one stage of late stage cell death where intracellular contents is released affecting neighboring cells and triggers the consequent inflammatory reaction [63]. However, the presented data did not show cells undergoing necrosis upon treatment with any thienopyrimidine analogue includes **7b**, indicating that cell death occurred primarily through early-stage apoptosis. Moreover, the highest potency of **7b** compared to other analogues and Raptinal may be suggested due to the potent inhibitory effect on glutamate release and mGluR-1 and this is consistent with other studies showing that mGluR-1 inhibitors inhibit tumor proliferation by inducing early apoptosis [8,9,23]. In addition, **7b** as well as other thienopyrimidines may alter different signaling

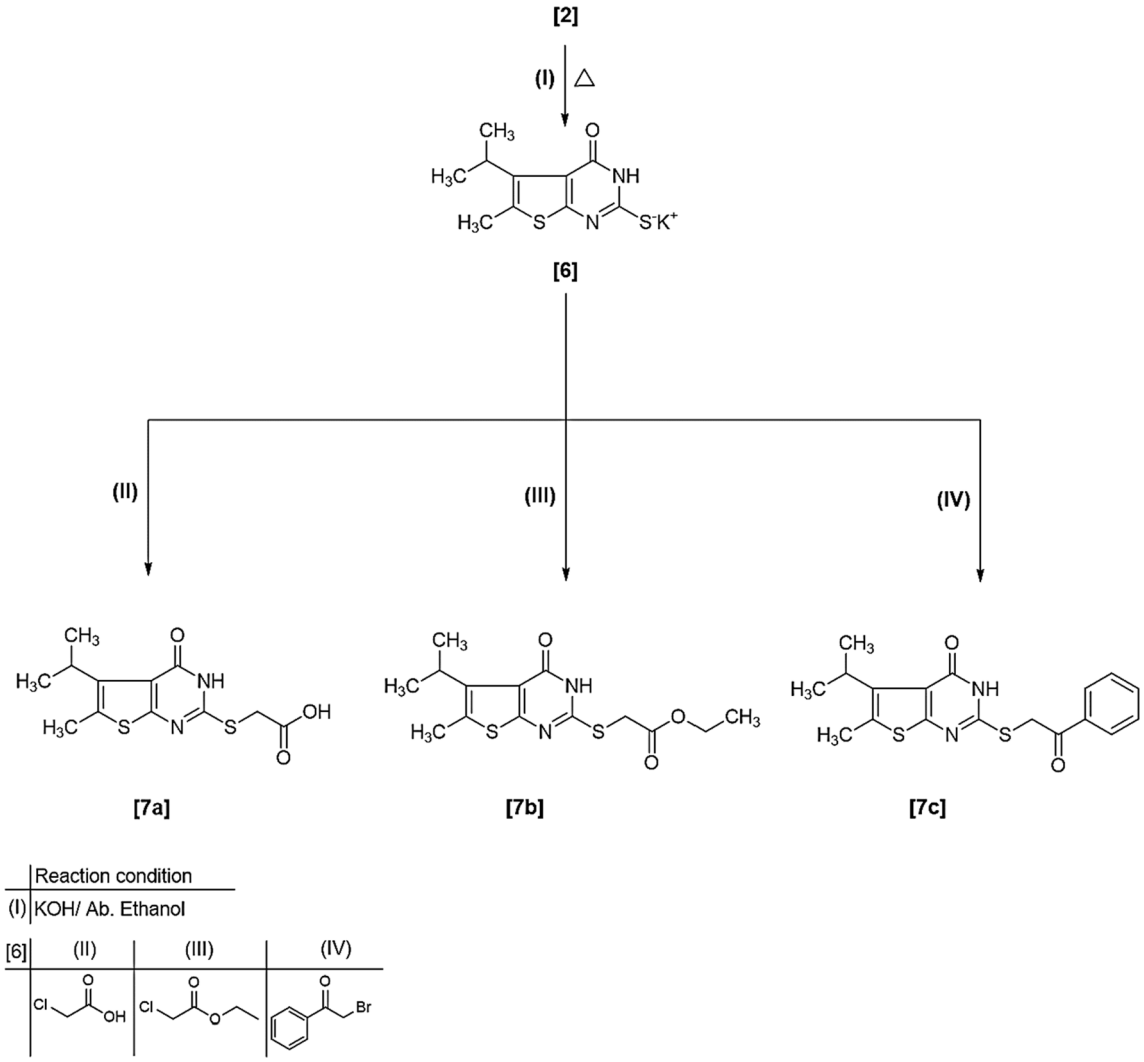

Scheme 4. Synthetic pathway for compounds; **7a-c.**

pathways that typically interfere with the balance between cell proliferation and apoptosis and shift MCF-7 cells toward the induction of apoptosis pathway [64]. This needs to be confirmed by changes in multiple signaling pathways of apoptosis to explain the apoptotic potency of **7b** on MCF-7 cell line.

2.2.5. Gene expression analysis for the effect of thienopyrimidine analogues in MCF-7 cells

Gene expression analysis was used for further assessment for key-related genes for mGluR-1 inhibitory and anticancer activity of the new thienopyrimidine. mGluR-1, SLC7A11 and key-related apoptotic pathway (FasL, FasL, TNF-α, Casp-3, Casp-8, Cyt-C, Bax, Bcl-2) were used in assessment. In this study, treatment of MCF-7 cells with antiproliferative IC_{50} was carried out for 24 hrs for thienopyrimidine analogues (**1′**, **2**, **3, 4a**, **5a**, **7a**, **7b**, **7c**, **8**, **4b**, **5b** and **9**).

2.2.5.1. Gene expression analysis of mGluR-1 and SLC7A11 genes in MCF-7 cells and effect on cell proliferation. It was essential to investigate and explain the potency of compound **7b** as m-GluR-1 inhibitor using mGluR-1 and SLC7A11 genes. Fig. 7A showed mGluR-1 gene expression was down-regulated after treatment with compounds **1′**, **2, 3, 7a**, **7b**, **7c**, **8, 4b**, however, Compound **7b** induced the lowest level of down-regulation as fold change (0.11) compared to control, Table 5. Additionally, Fig. 7A showed SLC7A11 gene was down-regulated significantly with only compounds **7a**, **7b** and preferntial decrease with compond **7b** as fold change compared to control (0.6 and 0.1 respectively, Table 5). mGluR-1 gene encodes a metabotropic glutamate receptor that functions by activating G-protein coupled receptors that responsible for glutamate release extracellulary [65]. Cystine/glutamate transporter xCT coded by SLC7A11 is essential for RAS-induced tumorigenicity by enhancing antioxidant glutathione synthesis through cycteine transport inside cancer cells with glutamate releae [66]. SLC7A11 was found to be essential for oncogenic KRAS-mediated transformation and *In-vitro* knock-down of SLC7A11 strongly impaired growth of well established tumor model [67–69]. In the present study, both down-regulation of mGluR-1 and SLC7A11, in addition to reduced glutamate release mediated significantly with compound **7b** may suggest its mGluR-1 inhibitory potency to glutamate release extracellulary and antiproliferative activity observed.

2.2.5.2. Gene expression analysis of apoptosis-related genes in MCF-7 cells and effect on cell proliferation. Impaired apoptosis is the major hallmark in cancer development and restricting the effectiveness of any cancer therapies [70]. Thus, the induction of apoptosis is useful strategy for any anticancer agent to reduce cell proliferation [71]. Apoptosis is triggered via two main pathways, extrinsic pathway (the death receptor) or the intrinsic pathway (mitochondrial) [72]. In present study; FasL and TNF-α (death receptors) were selected as genes of extrinsic apoptosis in MCF-7 cells [73].

Fig. 7B showed that **1′**, **2, 7a**, **5a**, **9**, **8**, **5b**, **4b**, **7b** were able to induce

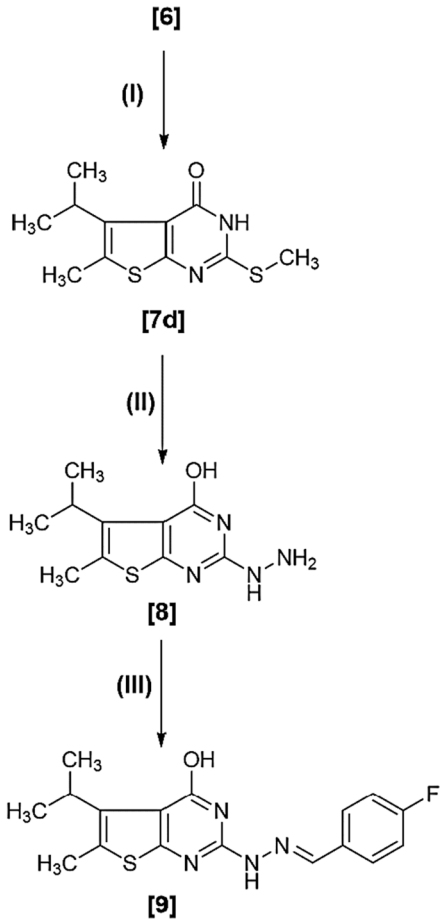

	Reaction condition
(I)	CH_3I
(II)	NH_2-$NH_2.H_2O$ / Abs. Ethanol / Dioxane (99%) (1:1)
(III)	Abs. Ethanol / few drops of piperidine

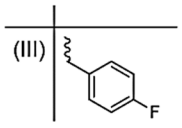

Scheme 5. Synthetic pathway for compounds; **7d**, **8**, and **9.**

the over-expression of FasL gene with variable potency with signficant elevation for compound **7b** compared to Raptinal apoptotic agent (Table 5). All previousely selected theinopyrimdine compounds were able to induce over-expression of TNF-α gene as second death receptor of extrinsic apoptosis (Fig. 7B). Table 5 showed compound **7b** was able to induced the signficant rised level of TNF-α followed by **7a** as fold change (105.4 and 55.7 respectively) compared to negative control, Raptinal and other selected compounds. TNF-α in MCF-7 cells sensitizes chemotherapy and radiotherapy via constitutive NF-κB activation and so render cells sensitive for apoptosis [74–76]. The potency of compound **7b** can be suggested due to enhanced induction of both FasL and TNF-α together compared to other compounds that induced one of the two death receptors.

For intrinsic pathway, the mitochondria is the starting point of initiation by releasing cytochrome -C (Cyt-C) into cytosol, assembling a multiprotein caspase-activating complex [77]. This complex is known as "apoptosome" that oligomerizes upon binding with Cyt-C then binds to procaspase-9 via interaction with its caspase recruitment domain [78]. This pathway is mainly activated by different apoptotic stimuli such as Raptinal [55], hence, it was selected as positive control and it induced Cyt-C overexpression as shown in Fig. 7B and Table 5 . Herein, Cyt-C expression levels was assessed to explore the adoption of mitochondrial intrinsic pathway after treatment with thienopyrimidine analogues. Fig. 7B showed expression level of Cyt-C was up-regulated after treatment with all the selected analogues suggesting their antiproliferative activity might be due to additional intrinsic pathway.

Table 5 showed compound **7b** induced exceptional elevated level of Cyt-C level (40.5) folds higher in MCF-7 cells compared to negative control and Raptinal treated cells (25.0) folds. Once cancer cells receiving specific signal instructions for undergoing apoptosis, it initiates a number of distinctive changes later on. Caspases (Casp), which are considered the real mediators in intrisic and extrinsic apoptosis [79], Caspases are activated at the early stages of apoptosis causing the different consequence of programmed cell death [80].

Caspase-3 (Casp-3) is known for its coordinating role in intrinsic apoptosis for destruction of cellular structures such as DNA fragmentation and degradation of cytoskeletal proteins [81]. On other side, caspase-8 (Casp-8) is required for extrinsic apotosis killing cancer cells

Table 1
Cytotoxicity assessment of the new synthesized thienopyrimidine compounds, Riluzole, 5-fluorouracil and Doxorubicin against different cancerous cell lines (MCF-7, A-549 and PC-3) and compared to WI-38 normal cell line. Corresponding SI (selectivity index) calculated as IC_{50} compound (WI-38)/ IC_{50} compound (cancer cell line). Data represent mean ± SEM, n = 3.

Compounds	*IC_{50} (μg/mL) ± SEM and corresponding SI						
	WI-38	MCF-7		A-549		PC-3	
	IC_{50}	IC_{50}	SI	IC_{50}	SI	IC_{50}	SI
Compounds with IC_{50} < 10 μg/mL							
7a	44.0 ± 6.60	7.50 ± 0.300	5.90	6.42 ± 0.700	6.90	11.3 ± 0.900	3.90
7b	68.0 ± 12.2	6.57 ± 0.200	10.4	6.31 ± 0.400	10.8	7.39 ± 0.500	9.20
Compounds with IC_{50} (10 ~ 50 μg/mL)							
1	75.0 ± 9.00	49.9 ± 1.60	1.50	30.2 ± 1.70	2.50	79.5 ± 2.70	0.600
1′	50.0 ± 10.0	30.8 ± 1.10	1.60	12.3 ± 0.800	4.10	56.8 ± 1.90	0.900
2	66.0 ± 11.2	29.7 ± 0.900	2.20	13.3 ± 0.900	5.00	45.1 ± 1.70	1.50
3	55.0 ± 13.4	28.2 ± 1.20	2.00	21.7 ± 0.600	2.50	27.4 ± 0.900	2.00
7c	73.0 ± 13.9	35.0 ± 1.20	2.10	19.1 ± 1.10	3.80	57.0 ± 2.70	1.30
8	88.0 ± 10.6	29.6 ± 1.10	3.00	49.3 ± 2.30	1.80	56.4 ± 2.60	1.60
4b	78.0 ± 10.9	27.4 ± 2.80	2.80	14.8 ± 0.840	5.30	36.7 ± 1.20	2.10
5b	83.0 ± 13.3	14.0 ± 0.84	5.90	7.10 ± 0.230	11.7	52.1 ± 2.70	1.60
9	49.0 ± 6.90	43.0 ± 3.60	1.10	35.9 ± 1.90	1.40	44.6 ± 2.3	1.10
Compounds with IC_{50} > 50 μg/mL							
2′	49.0 ± 6.40	71.4 ± 3.20	0.700	45.8 ± 1.90	1.10	124 ± 3.60	0.400
4a	37.0 ± 1.60	33.0 ± 1.30	1.10	19.0 ± 1.30	1.90	60.9 ± 1.80	0.600
5a	66.0 ± 6.70	120. ± 3.90	0.600	85.7 ± 3.20	0.800	198 ± 5.80	0.330
7d	49.0 ± 6.40	73.9 ± 3.50	0.700	47.4 ± 1.80	1.00	118 ± 3.10	0.410
5c	39.0 ± 4.30	121 ± 4.90	0.300	97.6 ± 3.70	0.400	172 ± 6.70	0.220
Standards							
Riluzole	75.0 ± 13.5	5.95 ± 0.900	12.6	27.5 ± 3.60	2.70	77.5 ± 2.30	0.970
5-Fluoruracil	>100	17.0 ± 1.90	>1	22.2 ± 1.10	>1	13.5 ± 2.70	>1
Doxorubicin	48.0 ± 8.20	6.80 ± 1.20	7.10	20.2 ± 3.20	2.40	8.00 ± 1.40	6.09

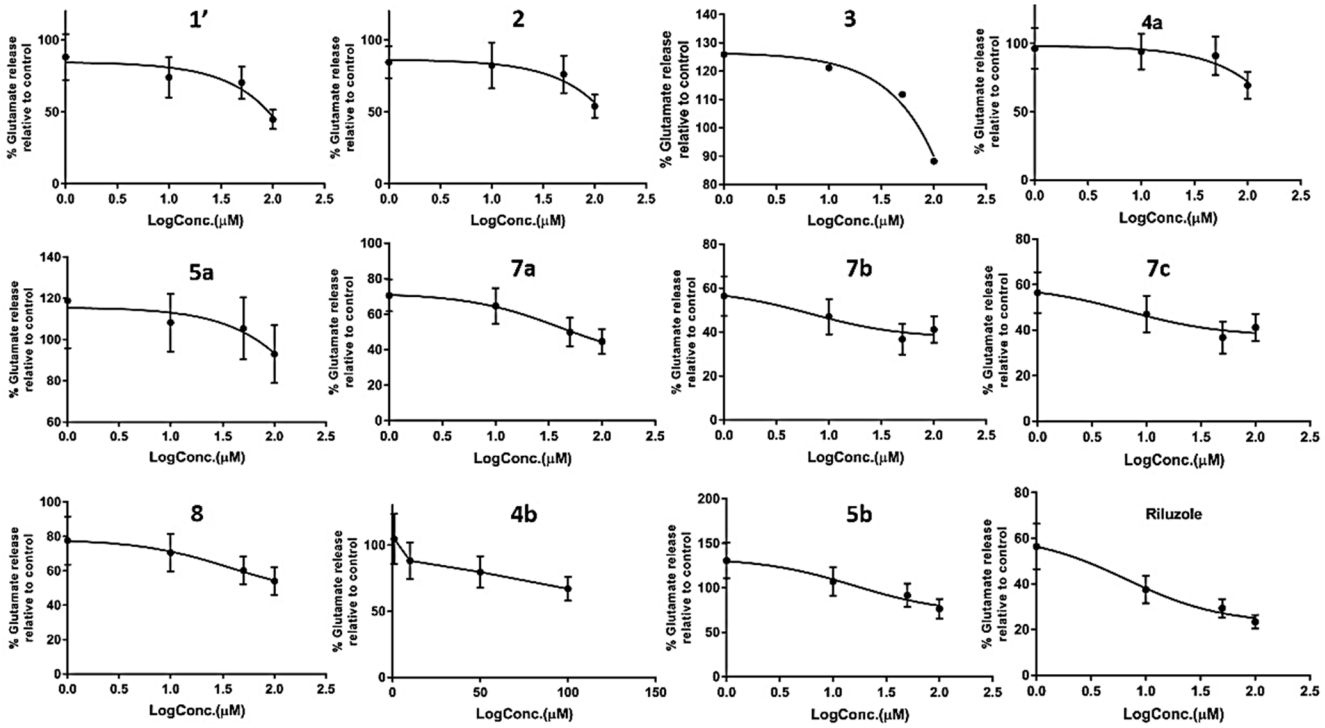

Fig. 3. IC_{50} curves of glutamate inhibition assay for the new synthetic thienopyrimidine analogues compared to Riluzole. The IC_{50} was calculated by normalizing to the negative control MCF-7 treated cells with 0.1% DMSO.

by the death receptors FasL, tumor necrosis factor receptor [82]. In this assay, the gene expression analysis of caspases -3 and -8 indicated that their activities were upregulated with most treated MCF-7 cells with antiproliferative IC_{50} concentration of the selected compounds for 24hrs (Fig. 7B) in consequence with the activation of FasL, TNF-α (extrinsic) and Cyt-C (intrinsic). Interstingly, compound **7b** as shown in Table 5, had the highest elevation in Casp-3 and -8 levels by 104.7 and 13.9 folds respectively comparing to the untreated MCF-7 cells and Raptinal positive control.

Finally, resistance of cancer cells can be mediated through two

Table 2
IC_{50} of the selected new synthesized thienopyrimidine compounds, Riluzole causing 50% inhibition of glutamate extracellular release in culture medium presented as μM. Conc. of extracellular glutamate measured for control MCF-7 treated cells with 0.1% DMSO was 30.0 ng/μl and all the synthetic compounds were tested to induce 50% inhibition of glutamate release (15.2 ng/μl ± 0.16).

Compounds	IC_{50} (μM) ± SEM
1′	91.2 ± 15.0
2	121 ± 19.0
3	208 ± 22.0
4a	185 ± 30.0
5a	462 ± 69.0
7a	52.7 ± 6.00
7b	4.96 ± 0.700
7c	248 ± 39.0
8	297 ± 32.0
4b	N/A
5b	N/A
9	N/A
Riluzole	2.80 ± 0.500

Table 3
Intracellular glutamate concentration measured at IC_{50} of each selected new synthesized thienopyrimidine compounds that produced 50% inhibition of glutamate extracellular release compared to Riluzole. Compound **7b** was similar in response to Riluzole in retaining higher concentration of intracellular glutamate at IC_{50} dose causing 50% inhibition of glutamate extracellular release in culture medium.

Compounds	Intracellular glutamate conc. (ng/μl ± SEM)
1′	21.6 ± 3.00
2	27.6 ± 4.00
3	25.3 ± 3.00
4a	25.7 ± 4.00
5a	24.0 ± 5.00
7a	31.7 ± 5.00
7b	31.7 ± 5.00
7c	37.1 ± 7.00
8	23.0 ± 3.00
4b	15.2 ± 3.00
5b	21.3 ± 4.00
9	18.2 ± 3.00
Riluzole	32.2 ± 5.00

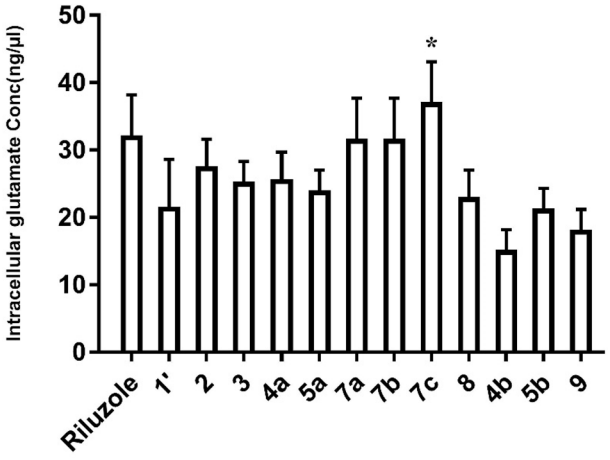

Fig. 4. Intracellular glutamate concentration measured at IC_{50} for each selected new synthetic thienopyrimidine analogues that induced 50% inhibition of extracellular glutamate release compared to Riluzole. **7c** showed significant increase in intracellular glutamate concentration at $^*p < 0.5$. Data are presented as Mean ± SEM.

countracting mediators; Bax and Bcl-2. The enhanced expression of Bcl-2 family genes in more than half of all cancers including MCF-7 cells is responsible for induction of hallmark cancer cell survival and become more resistant to many apoptotic stimuli including the most conventional anticancer drugs [83,84]. In turn the potent anticancer agents are those able to regulate the mitochondrial apoptotic pathway via reducing the anti-apoptotic gene effect of Bcl-2 by over-expressing intrinsic pro-apoptotic genes found on outer surface of mitochondria, such as Bax [85]. Accordingly, the gene expression analysis presented the impact of the selected thienopyrimidine analogues on expression of Bcl-2, Bax genes and the ratio of Bax/Bcl-2 as prognostic markers of MCF-7 apoptosis and diminshed resistance. Fig. 7C showed that compound **7b** was able to induce significant increase in level of Bax gene (2.1 fold change) followed by **7a** (1.4 fold change) compared to untreated control and other analogues and in a similar way to Raptinal control group (2.5), Table 5. Also, all selected DK-analogues did not induce down-regulation of Bcl-2 gene except compound **7b** which significantly induced its down-regulation to lowest level (0.82) comparable to Raptinal group. These results revealed that compound **7b** significantly boosted the Bax/Bcl-2 ratio to 2.6 folds higher than negative control and comparable to Raptinal.

In summary, overall gene expression analysis data of mGluR-1 and SLC7A11 in addition to the key-apoptotic releated genes suggest that compound **7b** was the most potent theinopyrimdine analogue followed by **7a**. The significant potency of compound **7b** is unique due to combined inhibition of glutamate receptors controlling glutamate release wih cysteine exchange and induction of extrnisic and intrinsic apototic pathways. For the other selected thienopyrimidine analogues from categories 2 and 3, the observed moderate anticancer activity is due to the induction of apoptosis either intrinsic or extrinsic pathways.

2.3. Computational studies

2.3.1. Molecular docking

Molecular docking helps in prediction of both the best orientation for each conformation to predict the binding mode to be compared with the reference ligand. There is a confirmed and reported correlation between the computed docking scores, affinity, and the predicted biological activity against the specific target. The crystal structure of Metabotropic glutamate receptor mGluR1 from human source in complex with an inhibitor with pdb code = 3KS9 was downloaded from protein data bank and used for docking. According to the docking results, the calculated free energy of binding values presented in (Table 6), compounds **7d**, **7a** and **7b** showed the top ranked docking scores with almost very close values; −19.11, −19.30, and −19.36 kcal/mol, respectively. The docking score of Riluzole (−19.46 kcal/mol) was similar to those of **7a** and **7b** that can be a good prediction for the biological activity of these two compounds. Compounds (**1**, **2**, **2′**, **5a**, **8**, **4b**, and **3**) showed scores in the same range of (−17.01 to −17.35 kcal/mol) and their biological activity was expected to be close to each other. The analysis and visualization of the docking poses of the different conformations of the docked compounds showed and confirmed some points. Compound **7a** formed a hydrogen bond by its C═O of the thienopyrimidinone moiety and Thr188, Ser165, Ala187. The sulfur atom from the side chain of **7a** formed another hydrogen bond with Ser165 (Fig. 8A).

Compound **7b** showed a common shared binding mode with Thr188 like **7a** with a hydrogen bond by its C═O of the thienopyrimidinone moiety and Thr188. The sulfur atom from the side chain of **7b** formed two hydrogen bonds with Ala187 and Ser165 (Fig. 8B). Compound **8** showed a hydrophobic interaction with its indole moiety and Thr188. In addition, the sulfur atom of the thiazole ring formed a hydrogen bond with the —OH of Tyr74 (Fig. 8C). Riluzole, was docked as a reference ligand to compare its binding mode with the tested compounds. It showed a unique interactions pose where it was the only ligand that formed hydrogen bonds with Arg203 and Asp474. Also. It showed a hydrogen bond with Ala187 (Fig. 8D).

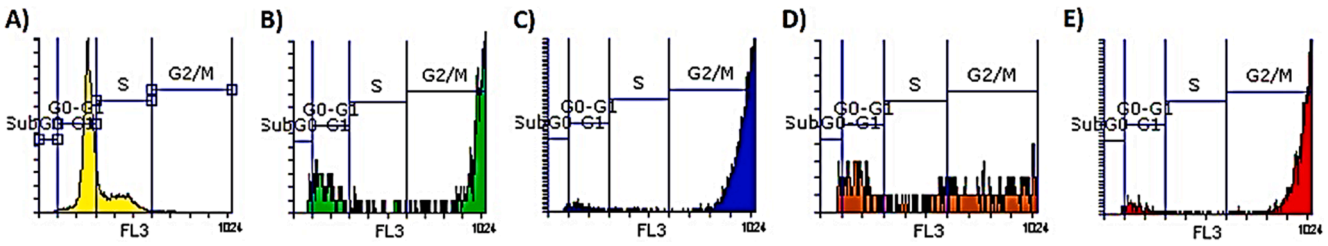

Fig. 5. Histograms of cell cycle analysis using Flow cytometry of treated MCF-7 cells for 24 hrs with; **A)** Negative control exposed to 0.1% DMSO solvent (yellow color), **B)** IC_{50} of **7b** (green color), **C)** IC_{50} of **7c** (blue color) , **D)** IC_{50} of **5c** (brown color) and **F)** IC_{50} of Raptinal positive control (red color). Histograms showing the phases of cell cycle arrest mainly at G_2M phase. **(color)**. (For interpretation of the references to color in this figure legend, the reader is referred to the web version of this article.)

Table 4
Summary for apoptosis assay and cell cycle analysis using flow cytometry of MCF-7 treated with 0.01% DMSO as control, IC_{50} of Raptinal, IC_{50} of thienopyrimidines analogues of **7a**, **7b**, and **5c** for 24 hrs. Table shows the percentage of cells in each cell cycle stage after treatment (viable, early apoptotic, late apoptotic, and necrotic). All thienopyrimidine analogues were able to significantly induce early apoptosis with G_2/M cell cycle arrest with **7b** was the most potent compound in inducing early cell apoptosis with significantly higher apoptotic index. AI was measured as percentage of early apoptotic cell events to the total cell events gated.

Cell cycle analysis MF-7 cells	Control cells	Raptinal	**7a**	**7b**	**5c**
% Gated Sub G_0-G_1 phase	0.250	0.0400	0.100	0.110	0.100
% Gated G_0-G_1 phase	68.0 ± 12.2	0.560	0.770	0.770	0.700
% Gated S phase	30.0 ± 6.00	0.200	0.350	0.250	0.400
% Gated G_2M phase	1.70 ± 0.300	99.2^{***} ±20.0	98.8^{***} ±17.0	98.9^{***} ±13.0	98.8^{***} ±20.0
% viable cells (C^{--})	80.3 ± 15.3	48.6^{**} ±7.00	31.1^{***} ±6.00	8.50^{***} ±2.00	21.1^{***} ±4.00
% early apoptotic cells (C^{+-})	19.6 ± 3.30	51.4^{***} ±8.00	68.9^{***} ±14.0	91.4^{***} ±16.0	78.8^{***} ±12.0
% late apoptotic cells (C^{-+})	0	0	0	0.0100	0
% necrotic cells (C^{++})	0.0800	0.100	0.0600	0.100	0.0900
%Apoptotic index (AI)	19.6	51.3	68.9	91.4	78.8

Data represent mean ± SEM, n = 3. *P*-values for comparison with control non-treated cells is $^{**}P < 0.01$, $^{***}P < 0.001$.

Compounds **1′**, **2**, **4a**, **8**, **4b**, and **3** showed a shared docking pose with Ser165 as they formed a hydrogen bond by either their C═O of the thienopyrimidinone ring (Fig. 9C and D) or the C═O of the ester of the side chain (Fig. 9A, C and 8E). A second hydrogen bond formed with Thr188 by compounds **1′**, **2**, **4a**, **4b** and **3** (Fig. 9A, B, C, E and F). The shared common binding mode of these compounds may be the reason for having a similar biological activity against MCF-7 cell line.

2.3.2. *Molecular dynamic simulations*

Molecular dynamic simulations (MD) were conducted to evaluate the stability and strength of binding for the top ranked compound (**7b**) and to compare it with the reference drug Riluzole. MD was performed over 20 ns for the best docked pose (ligand-protein complex) of both **7b** and Riluzole. The simulation of **7b** – protein complex showed its oscillations started at RMSD of 1.5 Å then increased till reached the equilibrium point at 2.5 Å after 6000 ps (Fig. 10A). On the other hand, Riluzole-protein complex reached the equilibrium point at RMSD of 2.00 Å after 8000 ps (Fig. 10B). Compound **7b** was faster in reaching the equilibrium point and achieving the stability than Riluzole however, it was achieved in slightly higher RMSD.

2.3.3. *Analysis of the least RMSD complex*

In order to investigate the lowest RMSD of (ligand-protein) complex that was reached just before the equilibrium point, the conformation of this complex was identified at Fig. 10A for further visualization and analysis of the ligand interactions of compound **7b**. The analysis resluts showed that compound **7b** was able to form two extra hydrogen bonds with two more residues Leu192 and Arg203 in addition to Ser165. Here it simulated Riluzole in interaction with Arg203 which confirms that Arg203 is an important residue that can predict the biological activity of any potential metabotropic glutamate receptors inhibitor from its ability to interact with Arg203 specially at the equilibrium point after MD simulations (Fig. 11).

2.3.4. *Analysis of the complex at equilibrium point 2.5 Å*

One complex of compound 7b-protein at RMSD 2.5 Å after achievement of equilibrium was analyzed as well to show the formed interactions at such point. It was found that compound 7b showed two hydrogen bonds with Ala187 and Arg203 and these are the two residues that riluzole formed interactions with. Compound 7b showed interactions with Ala187, Ser165 and Thr188 in docking results, then showed two interactions with Ser165 and Arg203 at the least RMSD during MD. Finally, it showed a pose where it formed interactions with Ala187 and and Arg203 like riluzole (Fig. 12).

3. Materials and methodds

3.1. *Chemistry*

Thin layer chromatography (TLC) was performed continuously by using Merck Alufolien Kieselgel 60 F_{254} Aluminum sheets, and visualization of spots under UV-lamp at λmax 254 nm. The used eluent was chloroform/methanol (9:1).

All melting points were measured on a Stuart melting point apparatus (SMP30) at National Research Centre, Cairo, Egypt and are uncorrected.

The Infrared (IR) spectra were recorded (KBr disk, ν cm^{-1}) on Jasco Fourier Transform Infrared Spectrometer FT/IR-6100 instrument in range 4000–400 cm^{-1} with resolution 4 cm^{-1} at National Research Centre, Cairo, Egypt.

^{1}H NMR Spectra were recorded on a Jeol ECA 500 MHz spectrophotometer at Central Laboratories, National Research Centre, Cairo, Egypt or on a Burker 400 MHz spectrometer at Microanalytical Unit-FOPCU- NMR Laboratory, Faculty of Pharmacy, Cairo University in deuterated dimethyl sulfoxide (DMSO-d_6) and the chemical shifts are expressed in (*ppm*) for δ scale. All coupling constant (*J*) values are reported in hertz.

^{13}C NMR Spectra were recorded on a Jeol ECA 125 MHz spectrometer at Central Laboratories, National Research Centre, Cairo, Egypt

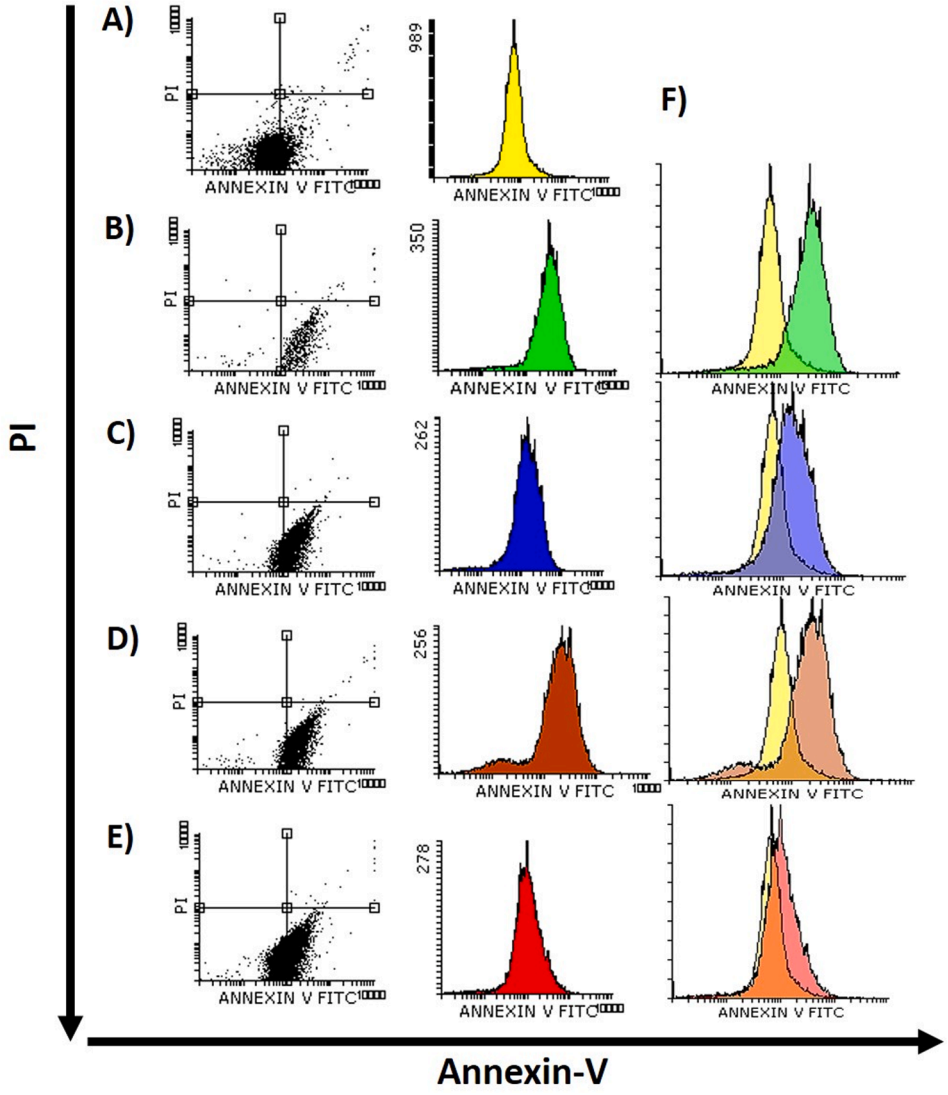

Fig. 6. Apoptosis analysis (annexin V-FITC/PI assay) of MCF-7 cells treated for 24 hrs with; **A)** Negative control exposed to 0.1% DMSO solvent (yellow histogram), **B)** IC_{50} of **7a** (green histogram), **C)** IC_{50} of **7b** (blue histogram), **D)** IC_{50} of **5c** (brown histogram) and **E)** IC_{50} of Raptinal as positive control (red histogram). **F)** Overly histograms of each synthetic thienopyrimidines and Raptinal compared to control and **7b** was shown to be the most potent compound able to induce shifting of cells to early apoptosis compared to Raptinal. **(color)**. (For interpretation of the references to color in this figure legend, the reader is referred to the web version of this article.)

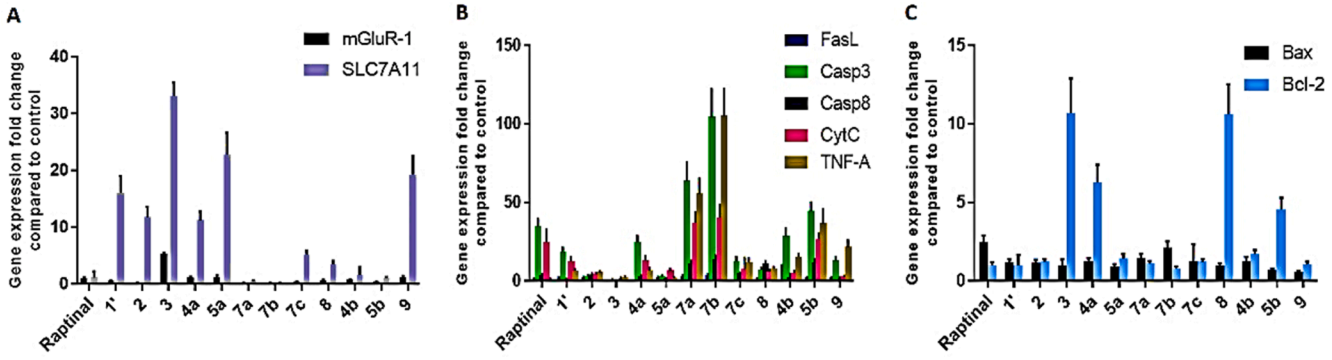

Fig. 7. Real-time quantitative PCR (qPCR) analysis of mRNA expression for different key genes suggested for controlling the pathways of the new synthetic thienopyrimidines ; **(A)** the metabotropic glutamate receptor and Cystine/glutamate antiporter xCT (SLC7A11) genes; **(B)** apoptosis regulatory markers for both intrinsic and extrinsic pathways and **(C)** intrinsic harmonic regulators of apoptosis in MCF-7 cells treated with IC_{50} dose of the selected new thienopyrimidine analogues for 24 hrs. Compound 4c was potent enough to induce significant down-regulation of mGluR-1 and SLC7A11 receptors that controlling the glutamate release. In addition, Compound **7b** was able to induce over-expression of both selected extrinsic (FasL, TNF-A Cap-8) and intrinsic (Casp-3 and Cyt-C) genes with over-expression of Bax and down-regulation of counteracting Bcl-2 gene. Quantification of target mRNA of genes were relative to negative control MCF-7 cells treated with 0.1% DMSO vehicle for the same time period and normalized to GAPDH. *P*-values for comparison with control non-treated cells is $^{**}P < 0.01$, $^{***}P < 0.001$. Figures on the data points represent the relative quantification compared to control. Data represent mean ± SEM, n = 3.

Table 5
Gene expression analysis of selected genes expressed as x-fold change for MCF-7 cells treated with IC_{50} of different thienopyrimidines for 24 hrs compared to negative control cells treated with 0.1% DMSO (RQ = Relative quantification). RAP = Raptinal.

Genes	Synthetic thienopyrimidines RQ, mean fold-change												
	1'	**2**	**3**	**4a**	**5a**	**7a**	**7b**	**7c**	**8**	**4b**	**5b**	**9**	**RAP**
Glutamate/Cysteine transporters													
mGluR-1	0.600	0.300	5.40	1.10	1.30	0.200	0.100	0.40	0.700	0.800	1.10	1.30	1.00
SLC7A11	16.1	11.8	33.1	11.2	22.8	0.600	0.100	5.20	3.50	1.60	11.2	19.3	1.20
Apoptotic genes													
FasL	1.80	2.30	0.200	0.200	2.30	3.30	3.80	0.200	1.30	1.50	2.10	1.90	1.20
TNF-α	6.50	5.60	2.30	6.90	2.10	55.7	105	11.9	7.90	15.7	36.8	21.9	1.20
Casp3	18.8	3.30	0.900	24.8	3.20	64.0	105	12.7	7.20	28.8	44.6	13.3	35.0
Casp8	1.20	4.10	0.100	2.80	1.70	11.1	13.9	4.80	11.0	2.40	11.8	1.70	3.50
Cyt-C	12.6	4.50	1.70	13.2	6.70	37.0	40.5	7.50	6.00	5.40	26.7	2.70	25.0
Bax	1.20	1.10	0.900	1.20	0.900	1.40	2.10	1.20	0.970	1.30	0.700	0.570	2.50
Bcl-2	4.00	1.20	10.7	6.30	1.40	1.10	0.820	1.20	10.6	1.70	4.60	1.10	1.00
Bax/Bcl-2	0.300	0.900	0.100	0.200	0.600	1.30	2.60	1.00	0.100	0.750	0.140	0.500	2.50

Table 6
Molecular docking results of the tested compounds using MOE 2016.08.

Compound	Free energy of binding kcal/mol	affinity	Interacted residues
1	−17.01	35.20	Ser165, Thr188
2	−17.22	35.73	Ser165, Thr188
2′	−17.18	35.65	Ser165, Thr188
4a	−17.24	35.94	Ser165, Thr188
5a	−16.95	33.12	Ser165, Thr188
7d	−19.11	44.02	Ser165, Thr188
7a	−19.30	44.21	Ser165, Thr188
7b	−19.36	44.25	Ser165, Thr188
7c	−17.03	35.35	Ser165, Thr188
8	−17.35	36.45	Ala187, Thr188
4b	−17.25	35.81	Ser165
5c	−16.75	33.95	Ser165, Thr188
5b	−16.55	33.71	Ser165, Thr188
9	−16.64	33.83	Ser165
3	−17.28	35.75	Ala187
Riluzole	−19.46	44.57	Asp474, Ala187, Arg203

or on a Burker 100 MHz spectrometer at Microanalytical Unit- FOPCU-NMR Laboratory, Faculty of Pharmacy, Cairo University in deuterated dimethyl sulfoxide (DMSO-d_6).

Mass spectra (MS) were performed on ISQ Single Quadrupole MS at Central Laboratories, National Research Centre, Cairo, Egypt.

Elemental analysis were carried out at the Micro Analytical Centre, Faculty of Science-Cairo University, Egypt.

3.1.1. Ethyl 2-amino-4-isopropyl-5-methylthiophene-3-carboxylate [1]

Preparation methods:

The starting material ethyl 2-amino-4-isopropyl-5-methylthiophene-3-carboxylate was prepared according to Karl Gewald Reaction (Version **II**).

Step-wise reaction:

A stirred mixture of methyl isobutyl ketone (10 ml, 1 mmole), ethyl cyanoacetate (11.3 ml, 1 mmole), diethylamine (7.3 ml, 1 mmole), absolute ethyl alcohol (20 ml) and sulfur powder (3.2 g, 1 mmole) was added portion wise to liquid mixture over a period of 1 hr. Continuous stirring of the mixture under water bath for (3–4 h., 40 °C). After this, let the reaction mixture to be in the room temperature overnight. The formed semi solid material was collected by shaking with petroleum ether (60–80 °C) then diethylether until solid substance was obtained. Solid substance was collected upon filtration, then dried, and crystallized from methyl alcohol to give grey powder **1** in low **yield** (40%, 0.9 g); **m.p.** 98–100 °C; **IR** (KBr, ν cm^{-1}): 3420, 3352 (—NH_2), 2995, 2880 (—CH, —CH_2, —CH_3), 1730 (—C═O), 1552 (—C═C); **^{1}H NMR** (DMSO-d_6, 400 MHz) δ *ppm*: 0.76 (d, J = 8 Hz, 3H, —C$\underline{H}_3$), 0.86 (d, J = 8 Hz, 3H, —C$\underline{H}_3$), 1.15–1.19 (t, J = 8 Hz, 3H, —C$\underline{H}_3$), 2.11 (s, 3H, —C$\underline{H}_3$), 2.91–2.98 (m, 1H, —C$\underline{H}$), 4.17–4.23 (q, J = 8 Hz, 2H, —C$\underline{H}_2$), 8.20 (br. s, 2H, —NH_2); **^{13}C NMR** (DMSO-d_6, 100 MHz) δ *ppm*: 11.02 (C$\underline{H}_3$), 15.1 (C$\underline{H}_3$), 22.5 (C$\underline{H}_3$), 22.6 (C$\underline{H}_3$), 27.8 (C$\underline{H}$), 58.0 (C$\underline{H}_2$), [112.0, 133.5, 137.6, 159.5, carbon atoms of thiophene ring], 171.0 (C═O); **EI-MS** *m/z* (%): 227 (M^+, 48.41%), 57.97 (100%); **Anal. Calcd. for $C_{11}H_{17}NO_2S$ (227.32)**: C, 58.06; H, 7.47; N, 6.15; S, 14.07%; **Found**: C, 58.02; H, 7.45; N, 6.11; S, 14.04%.

One-pot reaction:

Refluxing with stirring, methyl isobutyl ketone (10 ml, 1 mmole) was added to ethyl cyanoacetate (11.3 ml, 1 mmole), diethylamine (7.3 ml, 1 mmole), absolute ethyl alcohol (20 ml), and sulfur powder (3.2 g, 1 mmole) was added to liquid mixture under water bath (40 °C) over a period 3–4 h. The reaction mixture was cooled in the room temperature overnight. The formed crystals was collected, dried and crystallized from methyl alcohol as shiny grey crystals **1** with good **yield** (65%, 1.47 g); **m.p.** 101–103 °C. Compound **1** obtained from one-pot reaction has the same spectral analysis data, TLC, and m.p. of compound obtained from step-wise reaction, and with mixed melting point (98–101 °C).

3.1.2. Ethyl 4-isopropyl-5-methyl-2-thioureidothiophene-3-carboxylate [2′]

A mixture of product **1** (2.27 g, 10 mmole) was added to potassium thiocynate (0.97 g, 10 mmole), using 40 ml of dry dioxane as solvent, and 10 ml of concentrated hydrochloric acid was heated under reflux for 4–5 h. The reaction mixture was cooled and poured onto water. The formed precipitate was filtered off, washed thoroughly with water, let to dry and crystallized from dioxane to form **2′** as pale yellow powder in **yield** (60%, 1.71 g); **m.p.** 180–181 °C; **IR** (KBr, ν cm^{-1}): 3433, 3400 (—NH_2), 3330 (—NH—), 2920 (—CH, —CH_2, —CH_3), 1720 (—C═O), 1563 (—C═C); **^{1}H NMR** (DMSO-d_6, 400 MHz) δ *ppm*: 0.78 (d, J = 8 Hz, 3H, —C$\underline{H}_3$), 0.85 (d, J = 8 Hz, 3H, —C$\underline{H}_3$), 1.20–1.22 (t, J = 4 Hz, 3H, —C$\underline{H}_3$), 2.14 (s, 3H, —C$\underline{H}_3$), 2.88–2.96 (m, 1H, —C$\underline{H}$), 4.30–4.36 (q, J = 8 Hz, 2H, —C$\underline{H}_2$—) 9.61 (br. s, 2H, —NH_2), 10.32 (br. s, 1H, —NH); **^{13}C NMR** (DMSO-d_6, 100 MHz) δ *ppm*: 12.0 (C$\underline{H}_3$), 14.2 (C$\underline{H}_3$), 22.4 (C$\underline{H}_3$), 22.5 (C$\underline{H}_3$), 27.9 (C$\underline{H}$), 61.4 (C$\underline{H}_2$), [116.9, 135.1, 138.2, 157.5, carbon atoms of thiophene ring], 171.2 (C═O), 174.6 (C═S); **EI-MS** *m/z* (%): 286 (M^+, 29.75%), 63.93 (100%); **Anal. Calcd. for $C_{12}H_{18}N_2O_2S_2$ (286.41)**: C, 50.27; H, 6.28; N, 9.77; S, 22.34%; **Found**: C, 50.26; H, 6.25; N, 9.75; S, 22.31%.

3.1.3. 5-Isopropyl-2-mercapto-6-methylthieno[2,3-d]pyrimidin-4(3H)-one [2]

By addition of formed product **2′** (2.86 g, 10 mmole) to (2.5 g × 50

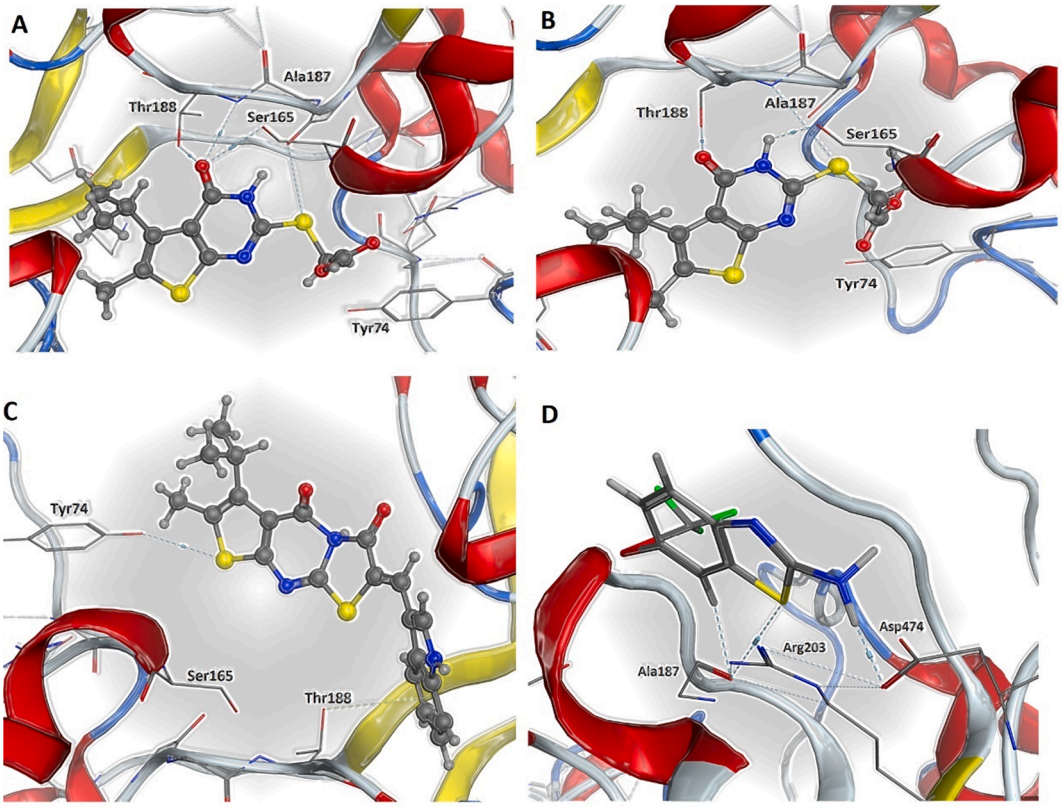

Fig. 8. The best docking pose of compounds: A) **7a** B) **7b** C) **8** and D) **Riluzole.**

ml water) of 5% sodium hydroxide, the mixture was heated till all the solid substance was completely dissolved. The mixture allow to cool and filtered off to collect all dissolved product then neutralizing using concentrated hydrochloric acid. The formed precipitate was filtered off, washed well with water several times, dried and crystallized from dioxane to form compound **2** as yellowish brown powder in **yield** (65%, 1.56 g); **m.p.** 189–190 °C; **IR** (KBr, ν cm^{-1}): 3301 (—NH—), 2924 (—CH, —CH_3), 1653 (—C═O), 1584 (—C═N), 1544 (—C═C); **^{1}H NMR** (DMSO-d_6, 400 MHz) δ *ppm*: 0.78 (d, J = 8 Hz, 3H, —C$\underline{H}_3$), 0.86 (d, J = 8 Hz, 3H, —C$\underline{H}_3$), 2.31 (s, 3H, —C$\underline{H}_3$), 2.84–2.92 (m, 1H, —C$\underline{H}$), 10.28 (br. s, 1H, —NH—); **^{13}C NMR** (DMSO-d_6, 100 MHz) δ *ppm*: 12.9 (C$\underline{H}_3$), 22.4 (C$\underline{H}_3$), 22.5 (C$\underline{H}_3$), 28.6 (C$\underline{H}$), [117.6, 135.0, 138.9, 157.8, 160.9, carbon atoms of thienopyrimidine ring system], 169.5 (C═O); **EI-MS** *m/z* (%): 240 (M^+, 100%), 111.14 (70.88%); **Anal. Calcd. for $C_{10}H_{12}N_2OS_2$ (240.34)**: C, 49.92; H, 4.99; N, 11.65; S, 26.62%; **Found**: C, 49.89; H, 4.98; N, 11.62; S, 26.58%.

3.1.4. 6-Isopropyl-7-methyl-5H-thiazolo[3,2-a]thieno[2,3-d]pyrimidine-3,5(2H)-dione [3]

A mixture of compound **2** (2.40 g, 10 mmole), chloroacetic acid (01.04 g, 10 mmole), and anhydrous sodium acetate (4.1 g, 50 mmole) in glacial acetic acid (50 ml) containing acetic anhydride (25 ml) was refluxed for 3–4 h with continuous stirring.

The formed precipitate was cooled and filtered off, washed well with water, dried and crystallized from dioxane, to give compound **3** as yellowish grey powder in **yield** (65%, 1.82 g); **m.p.** 180–182 °C; **IR** (KBr, ν cm^{-1}): 2955, 2858 (—CH, —CH_3), 1681 (—C═O), 1661 (—C═O), 1611 (—C═N), 1547 (—C═C); **^{1}H NMR** (DMSO-d_6, 500 MHz) δ *ppm*: 0.81 (d, J = 10 Hz, 3H, —C$\underline{H}_3$), 0.97 (d, J = 10 Hz, 3H, —C$\underline{H}_3$), 2.34 (s, 3H, —C$\underline{H}_3$), 2.82–2.89 (m, 1H, —C$\underline{H}$), 3.87 (s, 2H, —C$\underline{H}_2$—, active methylene proton); **^{13}C NMR** (DMSO-d_6, 125 MHz) δ *ppm*: 11.3 (C$\underline{H}_3$), 22.6 (2 C$\underline{H}_3$), 28.5 (C$\underline{H}$), 31.2 (C$\underline{H}_2$), 117.4, 132.8, 138.1, 157.2, 159.4, 170.2 (C═O), 172.4 (C═O); **EI-MS** *m/z* (%): 280 (M^+, 75.21%), 236.98(100%); **Anal. Calcd. for $C_{12}H_{12}N_2O_2S_2$ (280.36)**: C, 51.36; H, 4.28; N, 9.98; S, 22.82%; **Found**: C, 51.34; H, 4.24; N, 9.95; S, 22.79%.

*3.1.5. Preparation method for synthesis of compound **4a** and **4b***

A mixture of compound **2** (2.40 g, 10 mmole), chloroacetic acid (01.04 g, 10 mmole), anhydrous sodium acetate (4.1 g), and 10 mmole of aromatic aldehydes was used namely, 4-methoxybenzaldehyde and indole-3-carboxaldehyde was allowed to stirre under reflux in 50 ml of glacial acetic acid and 25 ml of acetic anhydride for 2–3 h. The formed precipitate was poured onto water, filtered off, dried and recrystallized from proper solvent to obtain **4a** and **4b** compounds.

3.1.6. 2-((5-Isopropyl-6-methyl-4-oxo-3,4-dihydrothieno[2,3-d]pyrimidin-2-yl)thio)-3-(4-methoxyphenyl)acrylic acid [4a]

Compound **4a** obtained from reaction of compound **2** (2.40 g, 10 mmole) and 4-methoxybenzaldehyde (1.36 g, 10 mmole). **Crystallization solvent**: Dioxane/DMF (1:1); as dark green powder in **yield** (60%, 2.49 g); **m.p.** 148–150 °C; **IR** (KBr, ν cm^{-1}): 3432 (broad, —OH), 3102 (—NH—), 2972, 2902 (—CH, —CH_3), 1721 (—C═O), 1660 (—C═O), 1598 (—C═N), 1545 (—C═C); **^{1}H NMR** (DMSO-d_6, 400 MHz) δ *ppm*: 0.81 (d, J = 8 Hz, 3H, —C$\underline{H}_3$), 0.90 (d, J = 8 Hz, 3H, —C$\underline{H}_3$), 2.34 (s, 3H, —C$\underline{H}_3$), 2.90–2.97 (m, 1H, —C$\underline{H}$), 3.91 (—OC$\underline{H}_3$), 7.31 (d, J = 8 Hz, 2H, Ar—H), 7.89 (d, J = 8 Hz, 2H, Ar—H), 8.03 (s, 1H, methine proton), 9.50 (br. s, 1H, —NH—), 12.72 (br. s, 1H, —OH); **^{13}C NMR** (DMSO-d_6, 100 MHz) δ *ppm*: 11.5 (C$\underline{H}_3$), 22.6 (2 C$\underline{H}_3$), 29.0 (C$\underline{H}$), 57.5 (OC$\underline{H}_3$) 110.5, 116.8 (2 C$\underline{H}$, Ar—C$\underline{H}$), 118.7, 130.4, 133.1 (2 C$\underline{H}$, Ar—C$\underline{H}$), [135.5, 138.7, 149.2, 155.3, 157.5, 159.2, aromatic-C], 170.0 (C═O), 172.0 (C$\underline{O}$OH); **EI-MS** *m/z* (%): 416 (M^+, 12.10%), 166.06 (100%); **Anal. Calcd. for $C_{20}H_{20}N_2O_4S_2$ (416.51)**: C, 57.62; H, 4.80; N, 6.72; S, 15.36%; **Found**: C, 57.59; H, 4.78; N, 6.71; S, 15.32%.

3.1.7. 3-(1H-Indol-3-yl)-2-((5-isopropyl-6-methyl-4-oxo-3,4-dihydrothieno[2,3-d]pyrimidin-2-yl)thio)acrylic acid [4b]

Compound **4b** obtained from reaction of compound **2** (2.40 g, 10 mmole) and indole-3-carboxaldehyde (1.45 g, 10 mmole).

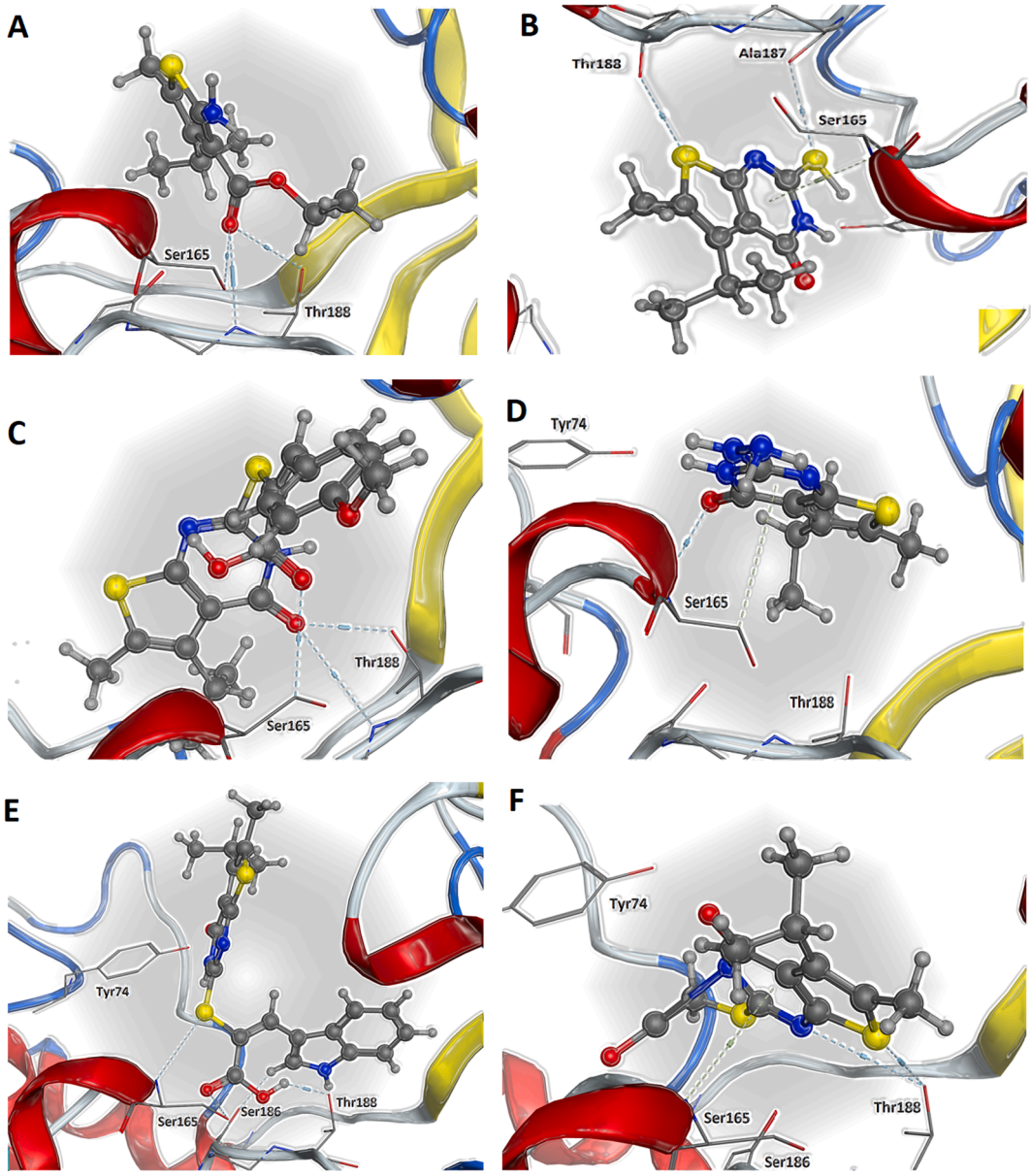

Fig. 9. The best docking pose of compounds: A) **1′**, B) **2,** C) **4a,** D) **8,** E) **4b and** F) **3.**

Crystallization solvent: Dioxane/DMF (3:1); as yellowish grey powder in **yield** (65%, 2.76 g); **m.p.** 264–266 °C; **IR** (KBr, ν cm^{-1}): 3431 (broad, —OH), 3271 (—NH—), 3203 (—NH—), 2924 (—CH, —CH_3), 1723 (—C═O), 1669 (—C═O), 1583 (—C═N), 1542 (—C═C); **^{1}H NMR** (DMSO-d_6, 500 MHz) δ *ppm*: 0.73 (d, J = 10 Hz, 3H, —C$\underline{H}_3$), 0.82 (d, J = 10 Hz, 3H, —C$\underline{H}_3$), 2.34 (s, 3H, —C$\underline{H}_3$), 2.80–2.88 (m, 1H, —C$\underline{H}$), 7.26–7.34 (m, 2H, Indole-H), 7.57 (d, J = 10 Hz, 1H, Indole-H), 8.14 (d, J = 10 Hz, 1H, Indole-H), 8.30 (d, J = 5 Hz, 1H, Indole-H), 8.67 (s, 1H, methine proton), 9.89 (br. s, 1H, —NH—), 10.83 (br. s, 1H, —NH—), 12.11 (br. s, 1H, —OH); **^{13}C NMR** (DMSO-d_6, 125 MHz) δ *ppm*: 11.6 (C$\underline{H}_3$), 22.6 (2 C$\underline{H}_3$), 28.6 (C$\underline{H}$), 111.5, 112.9, 115.0, 117.0, 121.3, 122.6, 123.9, 124.9, 133.0, 135.0, 138.9, 140.1, 147.5, 156.0, 158.5, 169.0 (C$\underline{=}$O), 170.5 (C$\underline{O}$OH); **EI-MS** *m/z* (%): 425 (M^+, 12.50%), 63.54 (100%); **Anal. Calcd. for $C_{21}H_{19}N_3O_3S_2$ (425.52)**: C, 59.22; H, 4.46; N, 9.87; S, 15.04%; **Found**: C, 59.21; H, 4.50; N, 9.83; S, 15.02%.

*3.1.8. General procedure for the synthesis of compounds **5a-c***

Method I (Two-step reaction): Addition of compound **3** (2.80 g, 10 mmole), anhydrous sodium acetate (4.1 g), was allowed to stirred under reflux in 50 ml of glacial acetic acid and 25 ml of acetic anhydride and 10 mmole of an aromatic aldehydes was used namely, 4-methoxybenzaldehyde, indole-3-carboxaldehyde or 4-hydroxy-3-nitrobenzaldehyde for 4–5 h. The precipitate was cooled and filtered off, washed well with water, dried and crystallized from appropriate solvent, to obtain **5a-c** compounds.

Method II (One-pot reaction): A mixture of compound **2** (2.40 g, 10 mmole), chloroacetic acid (01.04 g, 10 mmole), anhydrous sodium acetate (4.1 g), and 10 mmole of aromatic aldehydes was used namely, 4-methoxybenzaldehyde, indole-3-carboxaldehyde or 4-hydroxy-3-nitrobenzaldehyde was allowed to stirred under reflux in 50 ml of glacial acetic acid and 25 ml of acetic anhydride for 4–5 h. The reaction mixture was allowed to cool at room temperature and poured into water. The precipitate formed was filtered off, washed thoroughly with water, dried and recrystallized from suitable solvent, to obtain **5a-c** compounds with the same spectral data of method **I**.

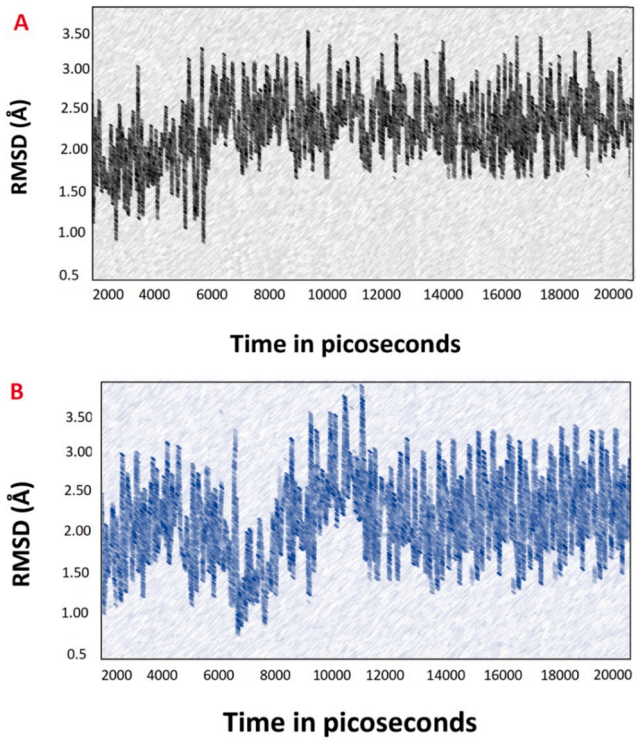

Fig. 10. A) Molecular dynamic simulation of Compound **7b** over 20 ns. B) Molecular dynamic simulation of Riluzole over 20 ns.

3.1.9. 6-Isopropyl-2-(4-methoxybenzylidene)-7-methyl-5H-thiazolo[3,2-a] thieno[2,3-d]pyrimidine-3,5(2H)-dione [5a]

Compound **5a** obtained from reaction of compound **2** (2.40 g, 10 mmole) or compound **3** (2.80 g, 10 mmole) and 4-methoxybenzaldehyde (1.36 g, 10 mmole).

Crystallization solvent: Dioxane/DMF (2:1); as yellowish green powder in **yield** (65%, 2.58 g) **yield**; **m.p.** 210–211 °C; **IR** (KBr, υ cm^{-1}): 2952, 2925 (—CH, —CH_3), 1671 (—C═O), 1652 (—C═O), 1582 (—C═N), 1551 (—C═C); **^{1}H NMR** (DMSO-d_6, 400 MHz) δ *ppm*: 0.89 (d, $J = 8$ Hz, 3H, —CH_3), 0.99 (d, $J = 8$ Hz, 3H, —CH_3), 2.31 (s, 3H, —CH_3), 2.90–2.98 (m, 1H, —CH), 3.87 (—OCH_3), 7.14 (d, $J = 8$ Hz, 2H, Ar—H), 7.88 (d, $J = 8$ Hz, 2H, Ar—H), 8.00 (s, 1H, methine proton); **^{13}C NMR** (DMSO-d_6, 100 MHz) δ *ppm*: 13.5 (CH_3), 22.6 (2 CH_3), 28.9 (CH), 56.0 (OCH_3) 114.6 (2 CH, Ar—CH), 115.6, 118.0, 128.0, 130.3 (2 CH, Ar-CH), [135.0, 137.8, 149.5, 156.3, 157.5, 159.9, aromatic-C], 170.3 (C═O), 172.2 (C═O); **EI-MS** *m/z* (%): 398 (M^+, 10.12%), 57.07 (100%); **Anal. Calcd. for $C_{20}H_{18}N_2O_3S_2$ (398.50)**: C, 60.22; H, 4.51; N, 7.02; S, 16.06%; **Found**: C, 60.21; H, 4.48; N, 6.98; S, 16.02%.

3.1.10. 2-((1H-Indol-3-yl)methylene)-6-isopropyl-7-methyl-5H-thiazolo [3,2-a]thieno[2,3-d]pyrimidine-3,5(2H)-dione [5b]

Compound **5b** obtained from reaction of compound **2** (2.40 g, 10 mmole) or compound **3** (2.80 g, 10 mmole) and indole-3-carboxaldehyde (1.45 g, 10 mmole). **Crystallization solvent**: Dioxane/DMF (1:1); as yellowish brown powder in **yield** (60%, 2.44 g); **m.p.** 153–155 °C; **IR** (KBr, υ cm^{-1}): 3229 (—NH—), 2926 (—CH, —CH_3), 1680 (—C═O), 1640 (—C═O), 1583 (—C═N), 1524 (—C═C);

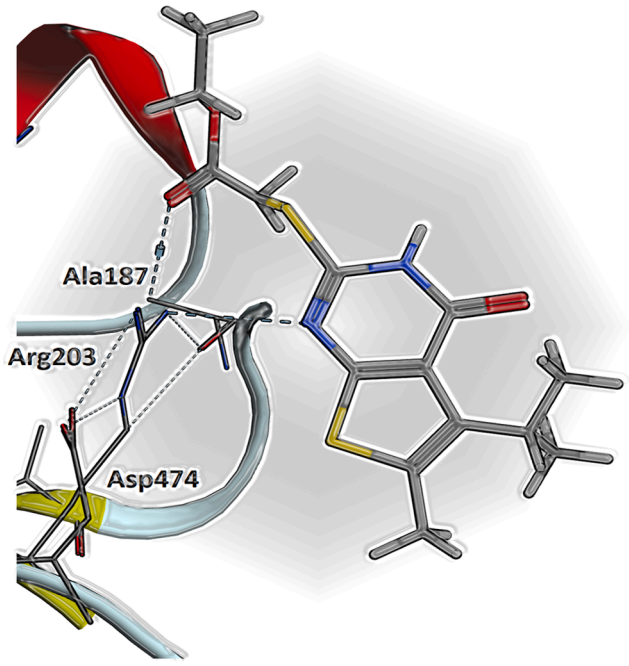

Fig. 12. The pose of compound 7b during equilibrium.

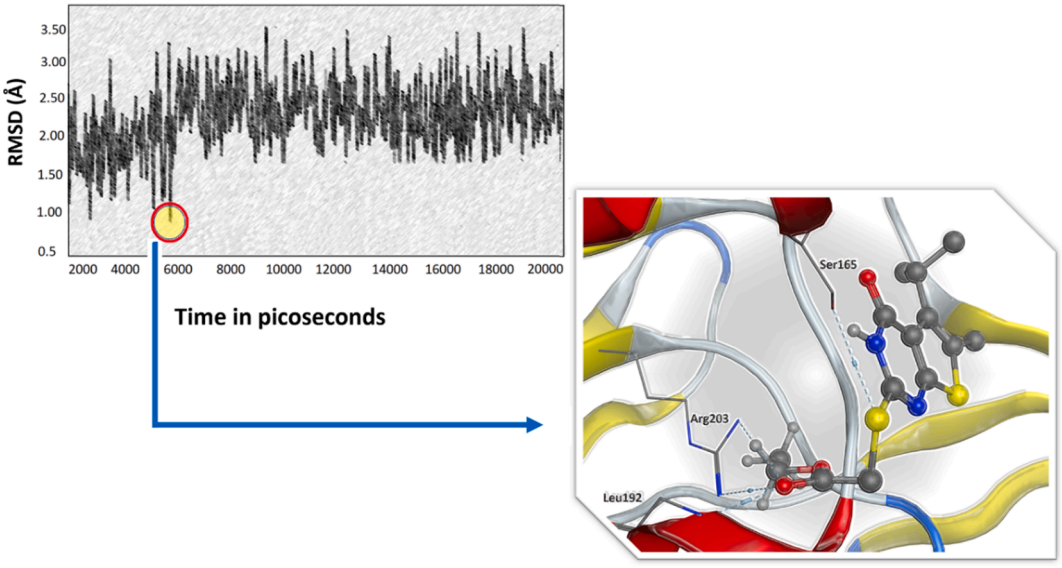

Fig. 11. The best MD pose with least RMSD during MD.

^{1}H NMR (DMSO-d_6, 500 MHz) δ *ppm*: 0.77 (d, J = 10 Hz, 3H, —C$\underline{H}_3$), 0.87 (d, J = 10 Hz, 3H, —C$\underline{H}_3$), 2.34 (s, 3H, —C$\underline{H}_3$), 2.82–2.90 (m, 1H, —C$\underline{H}$), 7.16–7.24 (m, 2H, Indole-H), 7.47 (d, J = 10 Hz, 1H, Indole-H), 8.05 (d, J = 10 Hz, 1H, Indole-H), 8.25 (d, J = 5 Hz, 1H, Indole-H), 8.66 (s, 1H, methine proton), 11.35 (br. s, 1H, —NH); **^{13}C NMR** (DMSO-d_6, 125 MHz) δ *ppm*: 12.2 (—$\underline{C}$H$_3$), 22.6 (2 $\underline{C}$H$_3$), 28.6 (—$\underline{C}$H), 111.3, 112.9, 118.7, 121.3, 122.6, 123.9, 124.6, 127.0, 129.0, 134.0, 137.5, 138.9, 145.2, 156.5, 158.3, 170.3 ($\underline{C}$=O), 172.1 ($\underline{C}$=O); **EI-MS** *m/z* (%): 407 (M^+, 10.40%), 144.01(100%); **Anal. Calcd. for $C_{21}H_{17}N_3O_2S_2$ (407.51)**: C, 61.83; H, 4.17; N, 10.30; S, 15.70%; **Found**: C, 61.81; H, 4.12; N, 10.28; S, 15.67%.

3.1.11. 2-(4-Hydroxy-3-nitrobenzylidene)-6-isopropyl-7-methyl-5H-thiazolo[3,2-a]thieno[2,3-d]pyrimidine-3,5(2H)-dione [5c]

Compound **5c** obtained from reaction of compound **2** (2.40 g, 10 mmole) or compound **3** (2.80 g, 10 mmole) and 4-hydroxy-3-nitrobenzaldehyde (1.67 g, 10 mmole). **Crystallization solvent**: Dioxane/DMF (1:1); as pale yellow powder in **yield** (65%, 2.78 g); **m.p.** 147–150 °C; **IR** (KBr, υ cm^{-1}): 3431 (broad, —OH), 2925 (—CH, —CH$_3$), 1680 (—C=O), 1665 (—C=O), 1597 (—C=N), 1531 (—C=C); **^{1}H NMR** (DMSO-d_6, 500 MHz) δ *ppm*: 0.82 (d, J = 7 Hz, 3H, —C$\underline{H}_3$), 0.98 (d, J = 7 Hz, 3H, —C$\underline{H}_3$), 2.34 (s, 3H, —C$\underline{H}_3$), 2.80–2.88 (m, 1H, —C$\underline{H}$), 7.14 (d, J = 10 Hz, 1H, Ar—H), 7.89 (d, J = 10 Hz, 1H, Ar-H), 8.30, (s, 1H, Ar-H), 8.57, (s, 1H, methine proton), 12.59 (br. s, 1H, —OH); **^{13}C NMR** (DMSO-d_6, 100 MHz) δ *ppm*: 13.0 ($\underline{C}$H$_3$), 22.5 (2 $\underline{C}$H$_3$), 28.7 ($\underline{C}$H), 117.3, 118.5, 119.4, 122.4, 129.0, 133.5, 135.4, 137.2, 138.7, 149.5, 155.0, 157.2, 159.2, 168.8 ($\underline{C}$=O), 172.0 ($\underline{C}$=O); **EI-MS** *m/z* (%): 429 (M^+, 9.52%), 212.00 (100%); **Anal. Calcd. for $C_{19}H_{15}N_3O_5S_2$ (429.47)**: C, 53.08; H, 3.49; N, 9.77; S, 14.90%; **Found**: C, 53.05; H, 3.47; N, 9.74; S, 14.89%.

*3.1.12. General procedure for the synthesis of compounds **7a-d***

A solution of ethanolic potassium hydroxide; (prepared by dissolving potassium hydroxide (0.56 g, 0.01 mmole) in 50 ml of absolute ethyl alcohol.)), was allowed for heating under reflux, left to cool at room temperature, then added (0.240 g, 0.01 mmole) of compound **2** and was continued heated under reflux, and the mixture was allowed to cool at room temperature. Then addition of 0.01 mmole of various alkylating agents was used namely, chloroacetic acid, ethyl chloroacetate, phenacyl bromide, and iodomethane, was stirred under reflux for 4–5 h. The mixture was allowed to cool at room temperature, then poured into water, the obtained precipitate was filtered off, dried and crystallized from proper solvent that gave different compounds **7a-d**.

3.1.13. 2-((5-Isopropyl-6-methyl-4-oxo-3,4-dihydrothieno[2,3-d]pyrimidin-2-yl)thio)acetic acid [7a]

From compound **2** (0.240 g, 0.01 mmole) and chloroacetic acid (0.94 g, 0.01 mmole). **Crystallization solvent**: Ethyl alcohol; as greenish brown powder in yield (60%, 1.78 g); **m.p.** 160–162 °C; **IR** (KBr, υ cm^{-1}): 3430 (broad, —OH), 3140 (—NH—), 2923 (—CH, —CH$_2$—, —CH$_3$), 1721 (—C=O), 1657 (—C=O), 1614 (—C=N), 1573 (—C=C); **^{1}H NMR** (DMSO-d_6, 400 MHz) δ *ppm*: 0.77 (d, J = 8 Hz, 3H, —C$\underline{H}_3$), 0.87 (d, J = 8 Hz, 3H, —C$\underline{H}_3$), 2.38 (s, 3H, —C$\underline{H}_3$), 2.86–2.94 (m, 1H, —C$\underline{H}$), 4.02 (s, 2H, —C$\underline{H}_2$—), 10.71 (br. s, 1H, —NH—), 12.74 (br. s, 1H, —OH); **^{13}C NMR** (DMSO-d_6, 100 MHz) δ *ppm*: 13.2 ($\underline{C}$H$_3$), 22.5 (2 $\underline{C}$H$_3$), 28.7 ($\underline{C}$H), 32.8 (CH$_2$), [117.3, 136.1, 138.0, 155.0, 158.9, carbon atoms of thienopyrimidine ring system], 168.8 ($\underline{C}$=O), 172.0 ($\underline{C}$OOH); **EI-MS** *m/z* (%): 298 (M^+, 10.63%), 238.94 (100%); **Anal. Calcd. for $C_{12}H_{14}N_2O_3S_2$ (298.38)**: C, 48.26; H, 4.69; N, 9.38; S, 21.44%; **Found**: C, 48.23; H, 4.65; N, 9.37; S, 21.42%.

3.1.14. Ethyl-2-((5-isopropyl-6-methyl-4-oxo-3,4-dihydrothieno[2,3-d]pyrimidin-2-yl)thio)acetate [7b]

From compound **2** (0.240 g, 0.01 mmole) and ethyl chloroacetate (0.112 g, 0.01 mmole). **Crystallization solvent**: Ethyl alcohol; as brownish green powder in yield (65%, 2.11 g); **m.p.** 125–127 °C; **IR** (KBr, υ cm^{-1}): 3311 (—NH—), 2924 (—CH, —CH$_2$—, —CH$_3$), 1734 (—C=O), 1660 (—C=O), 1593 (—C=N), 1522 (—C=C); **^{1}H NMR** (DMSO-d_6, 400 MHz) δ *ppm*: 0.77 (d, J = 8 Hz, 3H, —C$\underline{H}_3$), 0.86 (d, J = 8 Hz, 3H, —C$\underline{H}_3$), 1.21–1.25 (t, J = 8 Hz, 3H, C$\underline{H}_3$), 2.38 (s, 3H, —C$\underline{H}_3$), 2.84–2.92 (m, 1H, —C$\underline{H}$), 4.04 (s, 2H, —C$\underline{H}_2$—), 4.10–4.16 (q, J = 8 Hz, 2H, —C$\underline{H}_2$—), 10.74 (br. s, 1H, —NH—); **^{13}C NMR** (DMSO-d_6, 100 MHz) δ *ppm*: 13.2 ($\underline{C}$H$_3$), 14.5 ($\underline{C}$H$_3$), 22.5 (2 $\underline{C}$H$_3$), 28.7 ($\underline{C}$H), 32.8 ($\underline{C}$H$_2$), 61.5 ($\underline{C}$H$_2$—), [117.2, 133.1, 138.0, 154.5, 158.7, carbon atoms of thienopyrimidine ring system], 168.7 ($\underline{C}$=O), 172.8 ($\underline{C}$=O); **EI-MS** *m/z* (%): 326 (M^+, 38.96%), 57.09 (100%); **Anal. Calcd. for $C_{14}H_{18}N_2O_3S_2$ (326.43)**: C, 51.46; H, 5.51; N, 8.57; S, 19.60%; **Found**: C, 51.42; H, 5.48; N, 8.56; S, 19.57%.

3.1.15. 5-Isopropyl-6-methyl-2-((2-oxo-2-phenylethyl)thio)thieno[2,3-d]pyrimidin-4(3H)-one [7c]

From compound **2** (0.240 g, 0.01 mmole) and phenacyl bromide (0.119 g, 0.01 mmole). **Crystallization solvent**: Ethyl alcohol; as yellowish brown powder in **yield** (60%, 2.14 g); **m.p.** 68–70 °C; **IR** (KBr, υ cm^{-1}): 3223 (—NH—), 2922, 2857 (—CH, —CH$_2$—, —CH$_3$), 1715 (—C=O), 1655 (—C=O), 1598 (—C=N), 1544 (—C=C); **^{1}H NMR** (DMSO-d_6, 400 MHz) δ *ppm*: 0.83 (d, J = 8 Hz, 3H, —C$\underline{H}_3$), 0.94 (d, J = 8 Hz, 3H, —C$\underline{H}_3$), 2.37 (s, 3H, —C$\underline{H}_3$), 2.88–2.96 (m, 1H, —C$\underline{H}$), 4.74 (s, 2H, —C$\underline{H}_2$—), 7.48–7.70 (m, 3H, Ar—H), 8.01 (d, J = 8 Hz, 1H, Ar—H), 8.06 (d, J = 8 Hz, 1H, Ar—H) 11.50 (br. s, 1H, —NH—); **^{13}C NMR** (DMSO-d_6, 100 MHz) δ *ppm*: 13.2 ($\underline{C}$H$_3$), 22.5 (2 $\underline{C}$H$_3$), 28.7 ($\underline{C}$H), 38.4 ($\underline{C}$H$_2$), [117.0, 128.1, 128.5, 128.7, 129.2, 134.0, 134.3, 136.3, 137.9, 156.2, 158.8, carbon atoms of thienopyrimidine and aromatic rings], 165.1 ($\underline{C}$=O), 193.9 ($\underline{C}$=O); **EI-MS** *m/z* (%): 358 (M^+, 13.50%), 105.02 (100%); **Anal. Calcd. for $C_{18}H_{18}N_2O_2S_2$ (358.47)**: C, 60.25; H, 5.02; N, 7.81; S, 17.85%; **Found**: C, 60.24; H, 4.99; N, 7.79; S, 17.83%.

3.1.16. 5-Isopropyl-6-methyl-2-(methylthio)thieno[2,3-d]pyrimidin-4(3H)-one [7d]

From compound **2** (0.240 g, 0.01 mmole) and iodomethane (0.141 g, 0.01 mmole). **Crystallization solvent**: Dioxane; as yellowish grey powder in **yield** (65%, 1.65 g); **m.p.** 273–275 °C; **IR** (KBr, υ cm^{-1}): 3225 (—NH—), 2924 (—CH, —CH$_3$), 1655 (—C=O), 1599 (—C=N), 1540 (—C=C); **^{1}H NMR** (DMSO-d_6, 400 MHz) δ *ppm*: 0.78 (d, J = 4 Hz, 3H, —C$\underline{H}_3$), 0.87 (d, J = 4 Hz, 3H, —C$\underline{H}_3$), 2.23 (s, 3H, —C$\underline{H}_3$), 2.71 (s, 3H, —C$\underline{H}_3$), 2.90–3.06(m, 1H, —C$\underline{H}$) 10.66 (br. s, 1H, —NH—); **^{13}C NMR** (DMSO-d_6, 100 MHz) δ *ppm*: 11.0 ($\underline{C}$H$_3$), 13.3 ($\underline{C}$H$_3$), 22.5 (2 $\underline{C}$H$_3$), 28.2 ($\underline{C}$H), [118.0, 135.0, 136.8, 157.2, 159.0, carbon atoms of thienopyrimidine ring system], 169.5 ($\underline{C}$=O); **EI-MS** *m/z* (%): 253.98 (M^+, 100%), 238.91 (99.26%); **Anal. Calcd. for $C_{11}H_{14}N_2OS_2$ (254.37)**: C, 51.89; H, 5.50; N, 11.00; S, 25.16%; **Found**: C, 51.87; H, 5.47; N, 10.97; S, 25.15%.

3.1.17. 2-Hydrazinyl-5-isopropyl-6-methylthieno[2,3-d]pyrimidin-4-ol [8]

Addition of compound **7d** (2.54 g, 10 mmole), hydrazine hydrate (99%) (7.62 ml) with ratio (1:3), in the presence of 25 ml absolute ethyl alcohol and 25 ml dioxane and allow to heat under reflux for 3 h. The formed product filtered off, washed off with water, left to dry, and recrystallized from dioxane to give compound **8** as yellowish brown powder in **yield** (60%, 1.42 g); **m.p.** 130–132 °C; **IR** (KBr, υ cm^{-1}): 3441 (broad, —OH), 3245, 3201 (—NH$_2$), 3140 (—NH—), 2971 (—CH, —CH$_3$), 1598, (—C=N), 1544, (—C=C); **^{1}H NMR** (DMSO-d_6, 500 MHz) δ *ppm*: 0.82 (d, J = 10 Hz, 3H, —C$\underline{H}_3$), 0.97 (d, J = 10 Hz, 3H, —C$\underline{H}_3$), 2.34 (s, 3H, —C$\underline{H}_3$), 2.86–2.94 (m, 1H, —C$\underline{H}$), 6.95 (br. s, 2H, —NH$_2$), 9.76 (br. s, 1H, —NH—), 12.58 (br. s, 1H, —OH); **^{13}C NMR** (DMSO-d_6, 125 MHz) δ *ppm*: 13.3($\underline{C}$H$_3$), 22.6 (2 $\underline{C}$H$_3$), 28.8 ($\underline{C}$H), 116.9, 127.2, 138.1, 141.2, 156.8, 162.3; **EI-MS** *m/z* (%): 238 (M^+, 86.48%), 211.98 (100%); **Anal. Calcd. for $C_{10}H_{14}N_4OS$ (238.31)**: C, 50.35; H, 5.87; N, 23.49; S, 13.42%; **Found**: C, 50.33; H, 5.84; N, 23.48; S, 13.38%.

3.1.18. 2-(2-(4-Fluorobenzylidene)hydrazinyl)-5-isopropyl-6-methylthieno [2,3-d]pyrimidin-4-ol [9]

Mixture of compound **8** (2.38 g, 10 mmole), few drops of piperidine, absolute ethyl alcohol (30 ml), and 4-fluorobenzaldehyde (1.24 ml, 10 mmole), was heated under reflux for 3 h. The formed precipitate was filtered off, washed off with water, dried and recrystallized from ethyl alcohol to give compound **9** as brownish red crystals in **yield** (65%, 2.23 g); **m.p.** 70–72 °C; **IR** (KBr, υ cm^{-1}): 3434 (broad, —OH), 3103 (—NH—), 2911 (—CH, —CH_3), 1600 (—C=N), 1550 (—C=C); **^{1}H NMR** (DMSO-d_6, 500 MHz) δ *ppm*: 0.82 (d, J = 10 Hz, 3H, —CH_3), 0.98 (d, J = 10 Hz, 3H, —CH_3), 2.34 (s, 3H, —CH_3), 2.90–2.98 (m, 1H, —CH), 7.02 (dd, J = 35, 10 Hz, 2H, Ar-H), 7.64 (d, J = 10 Hz, 2H, Ar-H), 8.07 (s, 1H, methine proton), 10.39 (br. s, 1H, —NH—), 12.50 (br. s, 1H, —OH); **^{13}C NMR** (DMSO-d_6, 125 MHz) δ *ppm*: 13.4 (CH_3), 22.6 (2 CH_3), 28.9 (CH), 113.5 (2 CH, Ar-CH), 125.9, 127.2, 132.1(2 CH, Ar-CH), 134.3, 136.2, 137.6, 149.9, 155.1, 161.0, 165.0; **EI-MS** *m/z* (%): 344 (M^+, 15.01%), 77.06 (100%); **Anal. Calcd. for $C_{17}H_{17}FN_4OS$ (344.41)**: C, 59.23; H, 4.93; N, 16.25; S, 9.29%; **Found**: C, 59.19; H, 4.91; N, 16.24; S, 9.26%.

3.2. In-vitro anti-cancer activity assays

3.2.1. Thienopyrimidines solutions

All synthetic thienopyrimidines as well as standard controls (Doxorubicin, 5-Flurouracil (5-FU), Riluzole and Raptinal) were prepared in DMSO solution of molecular biology grade as 10 mM stock solutions, split into aliquots and stored at −20 °C in the dark. All reagents were purchased from Sigma-Aldrich otherwise stated.

3.2.2. Cell culture

All cancer cell lines (MCF-7, A-549 and PC-3) as well as WI-38 normal firbroblast cells were purchased from tissue culture unit at the holding company for the production of vaccines, sera, and drugs (VACSERA, Giza, Egypt) and stored at Helwan Structural Biology Center for Excellence (HSBR, Helwan, Egypt). Cells were grown and maintained in DMEM containing 10% (v/v) fetal bovine serum FBS, 1% (v/v) penicillin–streptomycin, L-glutamine, pyruvate sodium at 37 °C with 5% CO_2. Culture media were replaced every 2–3 days. Before each experiment, the cultures were checked for confluency up to 90% and were washed with phosphate-buffered saline (PBS, pH 7.4), detached with 0.25% trypsin–ethylenediaminetetraacetic acid (EDTA) solution, centrifuged at 1000 rpm for 5 min, followed by resuspension.

3.2.3. Antiproliferation and cytotoxicity evaluation using viability assay

Viability assay using MTT formazan reagent on cancer cell lines was used for assessment of anti-cancer activity of the new synthetic compounds [86]. The relative numbers of viable cancer cells upon treatment for 24 hrs was compared to negative control cells treated with 0.1% DMSO solvent. All the synthetic thienopyrimidine analogues as well as positive controls of standard anticancer agents (Riluzole, 5-FU, Doxorubicin) were evaluated at series concentrations ranged from (1–500 μg/mL) in triplicates. The optical density was read at 570 nm with a microplate reader (800TSUV Biotek ELISA Reader). Cytotoxicity assesment was perfomed by measuring percent of viable number of normal cells to the viable number of cancer cells and calculated as Selectivity Index (SI); the ratio of IC_{50} compound (WI-38)/ IC_{50} compound (cancer cell line). The higher the SI ratio, the more effective and safe a drug would be during *In-vivo* treatment for a given anticancer agent.

3.2.4. Glutamate inhibitory assay

Glutamate assay was performed using the Glutamate Assay Kit (Sigma-Aldrich, MAK004) where glutamate concentration was determined by enzymatic assay, which results in a colorimetric (450 nm) product, proportional to the glutamate present according to the protocol [8]. For determination of extracellular glutamate released, MCF-7 cells were seeded at 1 × 10^6 overnight in 6-well plates in L-glutamate/glutamine free DMEM media and then treated with four doses of selected synthetic thienopyrimidines and standard Riluzole (100, 50, 10 and 1 μM) for 24 hrs. Culture media was collected and 50 μl transferred to 96-well plate. 100 μl of glutamate enzyme mix was added to each well and the mixture was incubated for 30 min at 37 °C. Colored developed was measured using (800TSUV Biotek ELISA Reader). For determination of intracellular glutamate concentration, MCF-7 cells was treated with IC_{50} of selected synthetic thienopyrimidines and Riluzole measured from the previous step (concentration causing 50% inhibition of glutamate release relative to control un-treated cells). Cells were lysed using 100 μl Glutamate Assay Buffer and insoluble cell debris was then removed by centrifugation at 13,000*g* for 10 min. The supernatant was transferred to 10 KDa MWCO spin filter to remove the unnecessary proteins, fat, or particulates in the sample and then it was brought to a final volume of 50 μl with Glutamate Assay Buffer and transferred to 96-well plate. Finally, 100 μl of Reaction Mix was added to each well and the mixture was incubated for 30 min at 37 °C and measuring the colored developed coloremetry. For determination of glutamate concentration, it was essential to create glutamate standard curve using 0.1 M Glutamate Standard with different dilutions (0 (blank), 2, 4, 6, 8, and 10 nmole/well). Glutamate concentration was measured according to the manufacturer's instruction and as previousely documented [87–90], represented as;

$$Sa/Sv = C$$

Sa = Amount of glutamate in unknown sample (nmole) from standard curve.
Sv = Sample volume (μL) added into the wells.
C = Concentration of glutamate in sample

Glutamate molecular weight: 147.3 g/mole

$$X \text{ nmole}/50\ \mu l = X \text{ nmole}/\mu l$$

$$X \text{ nmole}/\mu L \times 147.3 \text{ ng/nmole} = X \text{ ng}/\mu L$$

3.2.5. Cell cycle analysis

MCF-7 Cell cycle arrest and distribution at different cell cycle phases ($SubG_0$-G_1, G_0-G_1, S, G_2/M) were assessed, using the Propidium Iodide Flow Cytometry Kit (Beckman Coulter) followed by flow cytometry analysis using Flowing software 2.5.1. The cell cycle phase distribution was determined by (Beckman Coulter Epics XL) showing the propidium iodide fluorescence intensity on FL3 [91].

3.2.6. Apoptosis assay

V-FITC apoptosis assay was performed using Annexin V-FITC/PI double staining detection kit (Beckman Coulter) [92]. Brifely, MCF-7 cells were incubated at a density of 1 × 10^6 cells per 25 cm^2 flask for 24 hrs before treatment with IC_{50} of selected new synthetic thienopyrimidine analogues and Raptinal positive control for another 24 hrs. Cells were detached and suspended in 50 μg /ml propidium iodide (PI) staining solution and 20 μg /ml RNaseA, minimum of 10,000 cells per sample was acquired and analyzed using (Beckman Coulter Epics XL) and Flowing software 2.5.1. Apoptotic index (AI) was calculated as the number of apoptotic events or cell deaths expressed as percentage of all cells present or all cells counted [93,94].

3.2.7. Quantitative real-time RT-qPCR analysis

MCF-7 cells were seeded on 6-well plates at density of 1 × 10^6 for 24 hrs and exposed to IC_{50} concentration of for different selected new thienopyrimidine analogues for 24 hrs. The cells were lysed with Direct-zol RNA Kit (Zymo Research, USA). Reverse transcription was performed using Reverse Transcription Kit (RevertAid Reverse Transcriptase, Thermo Fisher Scientific). HERA SYBR® Green qPCR master mix (Willowfort) was used to analyze gene amplification by quantitative RT-qPCR in triplicate, and gene expression was calculated as fold change

according to the $2^{-\Delta\Delta Ct}$ method. All primers were designed using Primer Premier 5.0 and sequences are listed in (Table 1 Supplementary). Real-time PCR (Rotor-GeneQ-QIAGEN) was used in analysis. Bax/Bcl2 ratio was calculated as the gene expression fold change of Bax/ gene expression fold change of Bcl-2 [95–97].

3.3. Computational studies

3.3.1. Molecular docking studies

The molecular docking studies were conducted using Molecular Operating Environment (MOE 2016.08) [98] package license was purchased from Chemical Computing Group Inc., Sherbooke St, Montreal, QC, Canada49. Triangle matcher was used as a placement method. Two rescoring were computed; rescoring 1 was selected as London dG. Rescoring 2 was selected as affinity. Force field was used as a refinement. The crystal structure of Metabotropic glutamate receptor mGluR1 (human source) in complex with an inhibitor (pdb code = 3KS9) was downloaded from protein data bank (https://www.rcsb.org). This protein was resolved by X-ray crystallography method with resolution = 1.9 Å and R-value = 0.241.

3.3.2. Molecular dynamics simulations for protein ligand complexes

The docking of compound **7b** revealed a stable pose that was kept in the active site. The protein geometries, electron density and temperature-related factors were prepared. All hydrogens were added, and energy minimization was calculated. Any foreign solvent molecules in the system were deleted; salt atoms were then added to the system to surround the biomolecular protein–ligand complex in a spherical shape. Sodium chloride was added in a 0.1 mol/L concentration. The cell dimensions were of 81.9 × 81.9 × 81.9 Å. The total number of molecules within the system was 19,321, 1.01 g/cm^3. Assisted Model Building with Energy Refinement 10: Extended Hückel Theory (Amber 10:EHT) was selected as a force field. The heat was adjusted in order to increase the temperature of the system from 0 to 300 K, which was followed by equilibration and production for 300 ps; cooling was then initiated until 0 K was reached. The simulation was conducted over a 20 ns period of time (20,000 ps).

4. Statistical analysis

Data were analyzed using GraphPad Prism 7.0. All Figures and Tables display mean with its corresponding standard error (SEM) for three independent experiments as indicated in the legends. Comparisons between groups were conducted with one-way ANOVA (based on data structure) at *P*-value as indicated in each experiment.

5. Conclusion

New series of thienopyrimidine analogues have been synthesized as mGluR-1 inhibitors. Subsequently, All the new derivatives were subjected to *In-vitro* anticancer evaluation against range of cancer cell lines (MCF-7, A-549, PC-3) and compared to WI-38 normal cell line using MTT technique for calculaion of IC_{50} and SI using doxorubicin, 5-Fluorurcil and Riluzole as astandard drugs. The compounds exhibited variable anticancer activity with IC_{50} values ranging from 6.70 to 121 μg/mL and classified into three major categories. Compound **7b** had the highest antiproliferative effect against three cancer cell lines without cytotoxicy to normal cell line. Furthermore, selected thienopyrimdine derivatives were evaluated for their mGluR-1 inhibitory activity through inhibiton of glutamate release and measuring intracellular glutamate in sensitive MCF-7 cell line. Compound **7b** stood out as the most potent analogue among all tested analogues with IC_{50} of glutamate rlease inhibitory assay comparable to Riluzole. Moreover, compound **7c** induced accumulation of intracellular glutamate which is a trigger for cellular apoptosis. Compound **7b** showed an evident for induction of apoptosis in MCF-7 through cell cycle arrest at G_2/M phase, in addition to a significant increase in the percentage of annexin V-FITC-positive apoptotic cells at early phase compared to untreated control and Raptinal apoptotic agent. On gene expression level, compound **7b** also showed enhanced expression of all apoptotic signals (FasL, TNF-α, Cyt-C, Casp-3, Casp-8 and Bax) and reduced expression of anti-apoptotic signals (Bcl-2). It significantly boosted Bax/Bcl-2 ratio in MCF-7 cells to 2.6 folds. These results suggest the potential use of compound **7b** as a promising anticancer agent in multiple cancer cell line including MCF-7. Docking of compound **7b** showed docking score −19.36 kcal/mol and affinity of 44.25 to mGluR-1 that was very close to Riluzole results; −19.46 kcal/mol and affinity of 44.57. MD simulations of **7b** over 20 ns reached the equilibrium after 6 ns and was faster than Riluzole that did it at 8 ns. The findings would be pioneer in literature about these series of thienopyrimidine analogues as scaffolds of mGluR-1 inhibitors. Future presectives are recommended including optimization of results on the protein level and using knock-down model to confirm the mGluR-1 mechanism. New synthetic analogues are on-progress currently for lead optimization and *In-vivo* screening using breast cancer animal model and clinical investigations.

6. Role of the funding source

This research did not receive any specific grant from funding agencies in the public, commercial, or not-for-profit sectors.

Declaration of Competing Interest

The authors declare that they have no known competing financial interests or personal relationships that could have appeared to influence the work reported in this paper.

Acknowledgments

Authors would like to thank Prof. Sameh Soror for giving us the opportunity to use the facilities/equipment available in HSBR laboratory.

Appendix A. Supplementary material

Supplementary data to this article can be found online at https://doi.org/10.1016/j.bioorg.2021.104729.

References

[1] M.J. Meegan, N.M. O'Boyle, Special Issue "Anticancer Drugs", Multidisciplinary Digital Publishing Institute, 2019.
[2] L. Falzone, S. Salomone, M. Libra, Evolution of cancer pharmacological treatments at the turn of the third millennium, Front. Pharmacol. 9 (2018) 1300, https://doi.org/10.3389/fphar.2018.01300.
[3] R.B. Mokhtari, T.S. Homayouni, N. Baluch, E. Morgatskaya, S. Kumar, B. Das, H. Yeger, Combination therapy in combating cancer, Oncotarget 8 (23) (2017) 38022–38043.
[4] X.J. Liu, M.W. Salter, Glutamate receptor phosphorylation and trafficking in pain plasticity in spinal cord dorsal horn, Eur. J. Neurosci. 32 (2) (2010) 278–289.
[5] C.S. Bonnet, A.S. Williams, S.J. Gilbert, A.K. Harvey, B.A. Evans, D.J. Mason, AMPA/kainate glutamate receptors contribute to inflammation, degeneration and pain related behaviour in inflammatory stages of arthritis, Ann. Rheum. Dis. 74 (1) (2015) 242–251.
[6] G. Littlejohn, E. Guymer, Modulation of NMDA receptor activity in fibromyalgia, Biomedicines 5 (2) (2017) 15–24.
[7] V. Pereira, C. Goudet, Emerging trends in pain modulation by metabotropic glutamate receptors, Front. Mol. Neurosci. 11 (2019) 464–486.
[8] J. Fazzari, H. Lin, C. Murphy, R. Ungard, G. Singh, Inhibitors of glutamate release from breast cancer cells; new targets for cancer-induced bone-pain, Sci. Rep. 5 (2015) 8380, https://doi.org/10.1038/srep08380.
[9] C.L. Speyer, J.S. Smith, M. Banda, J.A. DeVries, T. Mekani, D.H. Gorski, Metabotropic glutamate receptor-1: a potential therapeutic target for the treatment of breast cancer, Breast Cancer Res. Treat. 132 (2) (2012) 565–573.
[10] C.L. Speyer, A.H. Hachem, A.A. Assi, J.S. Johnson, J.A. DeVries, D.H. Gorski, Metabotropic glutamate receptor-1 as a novel target for the antiangiogenic treatment of breast cancer, PLoS ONE 9 (3) (2014), e88830, https://doi.org/10.1371/journal.pone.0088830.

[11] R. Crupi, D. Impellizzeri, S. Cuzzocrea, Role of metabotropic glutamate receptors in neurological disorders, Front. Mol. Neurosci. 12 (2019) 20–30.
[12] C.L. Vallerga, F. Zhang, J. Fowdar, A.F. McRae, T. Qi, M.F. Nabais, Q. Zhang, I. Kassam, A.K. Henders, L. Wallace, Analysis of DNA methylation associates the cystine–glutamate antiporter SLC7A11 with risk of Parkinson's disease, Nat. Commun. 11 (1) (2020) 1–10.
[13] H. Sato, M. Tamba, S. Okuno, K. Sato, K. Keino-Masu, M. Masu, S. Bannai, Distribution of cystine/glutamate exchange transporter, system xc−, in the mouse brain, J. Neurosci. 22 (18) (2002) 8028–8033.
[14] X. Liu, K. Olszewski, Y. Zhang, E.W. Lim, J. Shi, X. Zhang, J. Zhang, H. Lee, P. Koppula, G. Lei, Cystine transporter regulation of pentose phosphate pathway dependency and disulfide stress exposes a targetable metabolic vulnerability in cancer, Nat. Cell Biol. 22 (4) (2020) 476–486.
[15] H. Mollazadeh, E. Mohtashami, S.H. Mousavi, M. Soukhtanloo, M.M. Vahedi, A. Hosseini, A.R. Afshari, A. Sahebkar, Deciphering the role of glutamate signaling in glioblastoma multiforme: current therapeutic modalities and future directions, Curr. Pharm. Des. (2020), https://doi.org/10.2174/1381612826666200603132456.
[16] R.G. Ungard, System xC-mediated glutamate transport inhibition in cancer-induced bone pain, 2012.
[17] M.G. Nashed, M.D. Balenko, G. Singh, Cancer-induced oxidative stress and pain, Curr. Pain Headache Rep. 18 (1) (2014) 384, https://doi.org/10.1007/s11916-013-0384-1.
[18] R.M. Cerchio, Riluzole induces DNA double strand breaks in mGluR1 expressing human melanoma cells, Rutgers University-School of Graduate Studies (2018).
[19] E.P. Seidlitz, M.K. Sharma, Z. Saikali, M. Ghert, G. Singh, Cancer cell lines release glutamate into the extracellular environment, Clin. Exp. Metastasis 26 (7) (2009) 781–787.
[20] J.L. Teh, R. Shah, S. La Cava, S.C. Dolfi, M.S. Mehta, S. Kongara, S. Price, S. Ganesan, K.R. Reuhl, K.M. Hirshfield, Metabotropic glutamate receptor 1 disrupts mammary acinar architecture and initiates malignant transformation of mammary epithelial cells, Breast Cancer Res. Treat. 151 (1) (2015) 57–73.
[21] S.C. Dolfi, D.J. Medina, A. Kareddula, B. Paratala, A. Rose, J. Dhami, S. Chen, S. Ganesan, G. Mackay, A. Vazquez, Riluzole exerts distinct antitumor effects from a metabotropic glutamate receptor 1-specific inhibitor on breast cancer cells, Oncotarget 8 (27) (2017) 44639–44653.
[22] C.L. Speyer, M.A. Nassar, A.H. Hachem, M.A. Bukhsh, W.S. Jafry, R.M. Khansa, D. H. Gorski, Riluzole mediates anti-tumor properties in breast cancer cells independent of metabotropic glutamate receptor-1, Breast Cancer Res. Treat. 157 (2) (2016) 217–228.
[23] C. Zhang, X.-R. Yuan, H.-Y. Li, Z.-J. Zhao, Y.-W. Liao, X.-Y. Wang, J. Su, S.-S. Sang, Q. Liu, Anti-cancer effect of metabotropic glutamate receptor 1 inhibition in human glioma U87 cells: involvement of PI3K/Akt/mTOR pathway, Cell. Physiol. Biochem. 35 (2) (2015) 419–432.
[24] K. Akamatsu, M.-A. Shibata, Y. Ito, Y. Sohma, H. Azuma, Y. Otsuki, Riluzole induces apoptotic cell death in human prostate cancer cells via endoplasmic reticulum stress, Anticancer Res. 29 (6) (2009) 2195–2204.
[25] C.A. Zarate Jr, H.K. Manji, Riluzole in psychiatry: a systematic review of the literature, Expert Opin. Drug Metab. Toxicol. 4 (9) (2008) 1223–1234.
[26] R.G. Armando, D.L. Mengual Gómez, D.E. Gomez, New drugs are not enough-drug repositioning in oncology: An update, Int. J. Oncol. 56 (3) (2020) 651–684.
[27] S. Sperling, T. Aung, S. Martin, V. Rohde, M. Ninkovic, Riluzole: A potential therapeutic intervention in human brain tumor stem-like cells, Oncotarget 8 (57) (2017) 96697–96709.
[28] F.R. Tang, Agonists and antagonists of metabotropic glutamate receptors: anticonvulsants and antiepileptogenic agents? Curr. Neuropharmacol. 3 (4) (2005) 299–307.
[29] J. Fazzari, G. Singh, Effect of glutaminase inhibition on cancer-induced bone pain, Breast Cancer: Targets Therapy 11 (2019) 273–282.
[30] G. Mangalagiu, M. Ungureanu, G. Grosu, I. Mangalagiu, M. Petrovanu, New pyrrolo-pyrimidine derivatives with antifungal or antibacterial properties in vitro, Annales pharmaceutiques françaises (2001) 139–140.
[31] M. Modica, M. Santagati, A. Santagati, V. Cutuli, N. Mangano, A. Caruso, Synthesis of new [1, 3, 4] thiadiazolo [3, 2-a] thieno [2, 3-d] pyrimidinone derivatives with antiinflammatory activity, Pharmazie 55 (7) (2000) 500–502.
[32] C.J. Shishoo, V.S. Shirsath, I.S. Rathod, M.J. Patil, S.S. Bhargava, Design, synthesis and antihistaminic (H1) activity of some condensed 2-(substituted) arylaminoethyl-pyrimidin-4 (3H)-ones, Arzneimittelforschung 51 (03) (2001) 221–231.
[33] A.S. Oganisyan, A. Noravyan, I. Dzhagatspanyan, A. Akopyan, Condensed Thienopyrimidine Derivatives: Synthesis and Anticonvulsant Activity of a Series of New Pyrano (thiopyrano)[4′, 3′: 4, 5] thieno [2, 3-d] pyrimidines, Pharm. Chem. J. 35 (3) (2001) 127–129.
[34] M. Guetschow, K. Droessler, S. Leistner, Polycyclic azines with heteroatoms in the 1-and 3-position. 40. Synthesis of heterocyclic immunomodulators. 2. 3-Mercaptoalkylthieno (2, 3-d) pyrimidine-2, 4 (1H, 3H)-diones: synthesis and testing of immunostimulant activity, Archiv der Pharmazie 328(3) (1995) 231–234.
[35] A.S. Aly, Kh. M. Abu-zied, Alaa El-Din M. Gaafar, Facile Syntheses of some Thieno [2,3-d]pyrimidine derivatives, Phosphorus, Sulfur, Silicon, Related Elements 183; (2008) 3063–3078.
[36] K.M. Abu-Zied, A. Gaafar, A. Aly, Synthesis and reactions of some novel azolothienopyrimidines and thienopyrimido-as-triazines derivatives, Phosphorus, Sulfur, Silicon Related Elements 182 (2) (2007) 447–474.
[37] K.M. Abu-Zied, Synthesis and reactions of novel thienopyrimidine and thiazolothienopyrimidine derivatives, Phosphorus, Sulfur, Silicon Related Elements 182 (9) (2007) 2179–2191.
[38] H.-B. Yu, B.-Y. Zou, X.-L. Wang, M. Li, Investigation of miscellaneous hERG inhibition in large diverse compound collection using automated patch-clamp assay, Acta Pharmacol. Sin. 37 (1) (2016) 111–123.
[39] P. Wiji Prasetyaningrum, A. Bahtiar, H. Hayun, Synthesis and cytotoxicity evaluation of novel asymmetrical mono-carbonyl analogs of curcumin (AMACs) against Vero, HeLa, and MCF7 Cell Lines, Scientia Pharmaceutica 86(2) (2018) 25. doi.org/10.3390/scipharm86020025.
[40] O.O. Ogbole, P.A. Segun, A.J. Adeniji, In vitro cytotoxic activity of medicinal plants from Nigeria ethnomedicine on Rhabdomyosarcoma cancer cell line and HPLC analysis of active extracts, BMC Complement. Alternat. Med. 17 (1) (2017) 494–504.
[41] S.S. Willard, S. Koochekpour, Glutamate signaling in benign and malignant disorders: current status, future perspectives, and therapeutic implications, Int. J. Biol. Sci. 9 (7) (2013) 728–742.
[42] R.E. Sexton, A.H. Hachem, A.A. Assi, M.A. Bukhsh, D.H. Gorski, C.L. Speyer, Metabotropic glutamate receptor-1 regulates inflammation in triple negative breast cancer, Sci. Rep. 8 (1) (2018) 1–11.
[43] W.Y. Luo, S.Q. Xing, P. Zhu, C.G. Zhang, H.M. Yang, N. Van Halm-Lutterodt, L. Gu, H. Zhang, PDZ Scaffold Protein CAL Couples with Metabotropic Glutamate Receptor 5 to Protect Against Cell Apoptosis and Is a Potential Target in the Treatment of Parkinson's Disease, Neurotherapeutics 16 (3) (2019) 761–783.
[44] Z.-C. Ye, H. Sontheimer, Glioma cells release excitotoxic concentrations of glutamate, Cancer Res. 59 (17) (1999) 4383–4391.
[45] H.J. Lee, B.A. Wall, J. Wangari-Talbot, S. Chen, Regulation of mGluR1 expression in human melanocytes and melanoma cells, Biochim. Biophys. Acta (BBA)-Gene Regulatory Mechanisms 1819 (11–12) (2012) 1123–1131.
[46] J. Teh, S. Chen, mGlu Receptors and Cancerous Growth, Wiley Interdiscip Rev Membr Transp, Signal 1 (2) (2012) 211–220.
[47] J.Y. Lumeng, B.A. Wall, J. Wangari-Talbot, S. Chen, Metabotropic glutamate receptors in cancer, Neuropharmacology 115 (2017) 193–202.
[48] J. Teh, S. Chen, Metabotropic glutamate receptors and cancerous growth, Wiley Interdiscip. Rev.: Membr. Transport Signal. 1 (2) (2012) 211–220.
[49] J. Hoffmann, A. Charles, Glutamate and its receptors as therapeutic targets for migraine, Neurotherapeutics 15 (2) (2018) 361–370.
[50] R. Shiratori, K. Furuichi, M. Yamaguchi, N. Miyazaki, H. Aoki, H. Chibana, K. Ito, S. Aoki, Glycolytic suppression dramatically changes the intracellular metabolic profile of multiple cancer cell lines in a mitochondrial metabolism-dependent manner, Sci. Rep. 9 (1) (2019) 1–15.
[51] T. Pfeiffer, S. Schuster, S. Bonhoeffer, Cooperation and competition in the evolution of ATP-producing pathways, Science 292 (5516) (2001) 504–507.
[52] S.Y. Lunt, M.G. Vander Heiden, Aerobic glycolysis: meeting the metabolic requirements of cell proliferation, Annu. Rev. Cell Dev. Biol. 27 (2011) 441–464.
[53] A. Maus, G.J. Peters, Glutamate and α-ketoglutarate: key players in glioma metabolism, Amino Acids 49 (1) (2017) 21–32.
[54] M.K. Lemieszek, A. Stepulak, K. Sawa-Wejksza, A. Czerwonka, C. Ikonomidou, W. Rzeski, Riluzole inhibits proliferation, migration and cell cycle progression and induces apoptosis in tumor cells of various origins, Anti-Cancer Agents Med. Chem. (Formerly Current Medicinal Chemistry-Anti-Cancer Agents) 18 (4) (2018) 565–572.
[55] R. Palchaudhuri, M.J. Lambrecht, R.C. Botham, K.C. Partlow, T.J. Van Ham, K. S. Putt, L.T. Nguyen, S.-H. Kim, R.T. Peterson, T.M. Fan, A small molecule that induces intrinsic pathway apoptosis with unparalleled speed, Cell Reports 13 (9) (2015) 2027–2036.
[56] S. Heimer, G. Knoll, K. Schulze-Osthoff, M. Ehrenschwender, Raptinal bypasses BAX, BAK, and BOK for mitochondrial outer membrane permeabilization and intrinsic apoptosis, Cell Death Dis. 10 (8) (2019) 1–13.
[57] H. Amawi, C. Karthikeyan, R. Pathak, N. Hussein, R. Christman, R. Robey, C. R. Ashby Jr, P. Trivedi, A. Malhotra, A.K. Tiwari, Thienopyrimidine derivatives exert their anticancer efficacy via apoptosis induction, oxidative stress and mitotic catastrophe, Eur. J. Med. Chem. 138 (2017) 1053–1065.
[58] M. Kandeel, M. Kamal ABDELHAMEID, M.B. LABIB, Synthesis of some novel thieno [3, 2-d] pyrimidines as potential cytotoxic small molecules against breast cancer, Chem. Pharmaceut. Bull. (2013), 637–647.
[59] M.B. Labib, P.F. Lamie, Design, synthesis and biological evaluation of novel thiophene and theinopyrimidine derivatives as anticancer agents, Med. Chem. Res. 25 (11) (2016) 2607–2618.
[60] F.M. Alminderej, H.H. Elganzory, M.N. El-Bayaa, H.M. Awad, W.A. El-Sayed, Synthesis and cytotoxic activity of new 1, 3, 4-thiadiazole thioglycosides and 1, 2, 3-triazolyl-1, 3, 4-thiadiazole N-glycosides, Molecules 24 (20) (2019) 3738–3751.
[61] S.B. Kntayya, M.D. Ibrahim, N. Mohd Ain, R. Iori, C. Ioannides, A.F. Abdull Razis, Induction of apoptosis and cytotoxicity by isothiocyanate sulforaphene in human hepatocarcinoma HepG2 cells, Nutrients 10(6) (2018) 718-732.
[62] B.S. Cummings, R.G. Schnellmann, Measurement of cell death in mammalian cells, Curr. Protocols Pharmacol. 25(1) (2004) 12.8. 1-12.8. 22-51.
[63] S.Y. Proskuryakov, V.L. Gabai, Mechanisms of tumor cell necrosis, Curr. Pharm. Des. 16 (1) (2010) 56–68.
[64] J.M. Coppola, B.D. Ross, A. Rehemtulla, Noninvasive imaging of apoptosis and its application in cancer therapeutics, Clin. Cancer Res. 14 (8) (2008) 2492–2501.
[65] C.M. Niswender, P.J. Conn, Metabotropic glutamate receptors: physiology, pharmacology, and disease, Annu. Rev. Pharmacol. Toxicol. 50 (2010) 295–322.
[66] J.K. Lim, A. Delaidelli, S.W. Minaker, H.-F. Zhang, M. Colovic, H. Yang, G.L. Negri, S. von Karstedt, W.W. Lockwood, P. Schaffer, Cystine/glutamate antiporter xCT (SLC7A11) facilitates oncogenic RAS transformation by preserving intracellular redox balance, Proc. Natl. Acad. Sci. 116 (19) (2019) 9433–9442.
[67] X. Ji, J. Qian, S.J. Rahman, P.J. Siska, Y. Zou, B.K. Harris, M.D. Hoeksema, I. A. Trenary, C. Heidi, R. Eisenberg, xCT (SLC7A11)-mediated metabolic

reprogramming promotes non-small cell lung cancer progression, Oncogene 37 (36) (2018) 5007–5019.
[68] K. Hu, K. Li, J. Lv, J. Feng, J. Chen, H. Wu, F. Cheng, W. Jiang, J. Wang, H. Pei, Suppression of the SLC7A11/glutathione axis causes synthetic lethality in KRAS-mutant lung adenocarcinoma, J. Clin. Investig. 130 (4) (2020) 1752–1766.
[69] E. Panieri, P. Telkoparan-Akillilar, S. Suzen, L. Saso, The NRF2/KEAP1 Axis in the Regulation of Tumor Metabolism: Mechanisms and Therapeutic Perspectives, Biomolecules 10 (5) (2020) 791–819.
[70] J. Plati, O. Bucur, R. Khosravi-Far, Dysregulation of apoptotic signaling in cancer: molecular mechanisms and therapeutic opportunities, J. Cell. Biochem. 104 (4) (2008) 1124–1149.
[71] H.D. Ryoo, A. Bergmann, The role of apoptosis-induced proliferation for regeneration and cancer, Cold Spring Harbor Perspect. Biol. 4 (8) (2012), a008797.
[72] S. Fulda, K.-M. Debatin, Extrinsic versus intrinsic apoptosis pathways in anticancer chemotherapy, Oncogene 25 (34) (2006) 4798–4811.
[73] R. Jan, Understanding apoptosis and apoptotic pathways targeted cancer therapeutics, Adv. Pharmaceut. Bull. 9 (2) (2019) 205–218.
[74] X. Wu, M.-Y. Wu, M. Jiang, Q. Zhi, X. Bian, M.-D. Xu, F.-R. Gong, J. Hou, M. Tao, L.-M. Shou, TNF-α sensitizes chemotherapy and radiotherapy against breast cancer cells, Cancer Cell Int. 17 (1) (2017) 13–24.
[75] D. Yan, N. Qin, H. Zhang, T. Liu, M. Yu, X. Jiang, W. Feng, J. Wang, B. Yin, T. Zhang, Expression of TNF-α leader sequence renders MCF-7 tumor cells resistant to the cytotoxicity of soluble TNF-α, Breast Cancer Res. Treat. 116 (1) (2009) 91–102.
[76] M.E. Burow, C.B. Weldon, Y. Tang, G.L. Navar, S. Krajewski, J.C. Reed, T. G. Hammond, S. Clejan, B.S. Beckman, Differences in susceptibility to tumor necrosis factor α-induced apoptosis among MCF-7 breast cancer cell variants, Cancer Res. 58 (21) (1998) 4940–4946.
[77] D. Chauhan, T. Hideshima, S. Rosen, J.C. Reed, S. Kharbanda, K.C. Anderson, Apaf-1/cytochrome c-independent and Smac-dependent induction of apoptosis in multiple myeloma (MM) cells, J. Biol. Chem. 276 (27) (2001) 24453–24456.
[78] M.H. Nazmy, R.A. Mekheimer, M.E. Shoman, M. Abo-Elsebaa, M. Abd-Elmonem, K. U. Sadek, Densely functionalized cinnolines: Controlled microwave-assisted facile one-pot multi-component synthesis and in vitro anticancer activity via apoptosis induction, Bioorg. Chem. 103932 (2020).
[79] K.M. Boatright, G.S. Salvesen, Mechanisms of caspase activation, Curr. Opin. Cell Biol. 15 (6) (2003) 725–731.
[80] G.M. Cohen, Caspases: the executioners of apoptosis, Biochem. J 326 (1) (1997) 1–16.
[81] M.O. Hengartner, The biochemistry of apoptosis, Nature 407 (6805) (2000) 770–776.
[82] S. Wang, W.S. El-Deiry, TRAIL and apoptosis induction by TNF-family death receptors, Oncogene 22 (53) (2003) 8628–8633.
[83] R.-A. Wang, Z.-S. Li, Q.-G. Yan, X.-W. Bian, Y.-Q. Ding, X. Du, B.-C. Sun, Y.-T. Sun, X.-H. Zhang, Resistance to apoptosis should not be taken as a hallmark of cancer, Chinese J. Cancer 33 (2) (2014) 47–50.
[84] M. Hassan, H. Watari, A. AbuAlmaaty, Y. Ohba, N. Sakuragi, Apoptosis and molecular targeting therapy in cancer, Biomed Res. Int. 2014 (2014), https://doi.org/10.1155/2014/150845.
[85] M.H. Kang, C.P. Reynolds, Bcl-2 inhibitors: targeting mitochondrial apoptotic pathways in cancer therapy, Clin. Cancer Res. 15 (4) (2009) 1126–1132.
[86] H. Haffez, H. Taha, M.A. Rabie, S.M. Awad, Y.M. Zohny, Synthesis, biological evaluation and molecular docking studies of novel thiopyrimidine analogue as apoptotic agent with potential anticancer activity, Bioorg. Chem. (2020), 104249, https://doi.org/10.1016/j.bioorg.2020.104249.
[87] Z. Zhang, J. Liu, C. Fan, L. Mao, R. Xie, S. Wang, M. Yang, H. Yuan, X. Yang, J. Sun, The GluN1/GluN2B NMDA receptor and metabotropic glutamate receptor 1 negative allosteric modulator has enhanced neuroprotection in a rat subarachnoid hemorrhage model, Exp. Neurol. 301 (2018) 13–25.
[88] C. Zhu, Q. Xu, C. Wang, Z. Mao, N. Lin, Evidence that CA3 is underling the comorbidity between pain and depression and the co-curation by Wu-Tou decoction in neuropathic pain, Sci. Rep. 7 (1) (2017) 1–14.
[89] P.-S. Mishra, K. Vijayalakshmi, A. Nalini, T. Sathyaprabha, B. Kramer, P.A. Alladi, T. Raju, Etiogenic factors present in the cerebrospinal fluid from amyotrophic lateral sclerosis patients induce predominantly pro-inflammatory responses in microglia, J. Neuroinflamm. 14 (1) (2017) 1–18.
[90] L. Polletta, E. Vernucci, I. Carnevale, T. Arcangeli, D. Rotili, S. Palmerio, C. Steegborn, T. Nowak, M. Schutkowski, L. Pellegrini, SIRT5 regulation of ammonia-induced autophagy and mitophagy, Autophagy 11 (2) (2015) 253–270.
[91] Y. Lei, H. Gan, Y. Huang, Y. Chen, L. Chen, A. Shan, H. Zhao, M. Wu, X. Li, Q. Ma, Digitoxin inhibits proliferation of multidrug-resistant HepG2 cells through G2/M cell cycle arrest and apoptosis, Oncol. Lett. 20(4) (2020) 1–1.
[92] Y. Ji, M. Yu, Z. Qi, D. Cui, G. Xin, B. Wang, W. Jia, L. Chang, Study on apoptosis effect of human breast cancer cell MCF-7 induced by lycorine hydrochloride via death receptor pathway, Saudi Pharmaceut. J. 25 (4) (2017) 633–637.
[93] S.H. Merchant, N.J. Gonchoroff, R.E. Hutchison, Apoptotic index by Annexin V flow cytometry: adjunct to morphologic and cytogenetic diagnosis of myelodysplastic syndromes, Cytometry: J. Int. Soc. Anal. Cytol. 46 (1) (2001) 28–32.
[94] C.S. Potten, What is an apoptotic index measuring? A commentary, Br. J. Cancer 74 (11) (1996) 1743–1748.
[95] H. Perlman, X. Zhang, M.W. Chen, K. Walsh, R. Buttyan, An elevated bax/bcl-2 ratio corresponds with the onset of prostate epithelial cell apoptosis, Cell Death Differ. 6 (1) (1999) 48–54.
[96] H. Azimian, M. Dayyani, M.T.B. Toossi, M. Mahmoudi, Bax/Bcl-2 expression ratio in prediction of response to breast cancer radiotherapy, Iranian J. Basic Med. Sci. 21 (3) (2018) 325–332.
[97] E. Khodapasand, N. Jafarzadeh, F. Farrokhi, B. Kamalidehghan, M. Houshmand, Is Bax/Bcl-2 ratio considered as a prognostic marker with age and tumor location in colorectal cancer? Iranian Biomed. J. 19 (2) (2015) 69–75.
[98] C.C.G. Inc., Molecular operating environment (MOE), Chemical Computing Group Inc 1010 Sherbooke St. West, Suite# 910, Montreal, QC, Canada, 2016.